PREPARATION AND CHARACTERIZATION OF SINGLE AND BILAYERED Ni- Ni-W STRIPS BY A P/M ROUTE

by

DIBYENDU BHATTACHARYYA
Y3106007

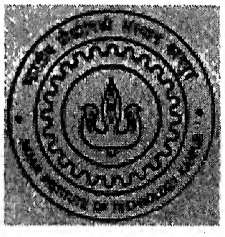

DEPARTMENT OF MATERIALS AND METALLURGICAL ENGINEERING
INDIAN INSTITUTE OF KANPUR
JUNE 2005

PREPARATION AND CHARACTERIZATION OF SINGLE AND BILAYERED Ni- Ni-W STRIPS BY A P/M ROUTE

A Thesis Submitted
In Partial Fulfillment of the Requirements
for the degree of
Master of Technology

by

DIBYENDU BHATTACHARYYA
Y3106007

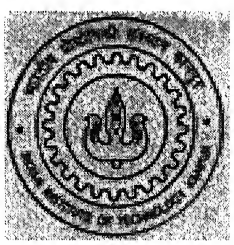

to the

DEPARTMENT OF MATERIALS AND METALLURGICAL ENGINEERING
INDIAN INSTITUTE OF KANPUR
JUNE 2005

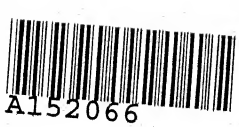

CERTIFICATE

This is to certify that the work contained in the thesis entitled "Preparation and characterization of single and bilayered Ni-Ni-W strips by a P/M route" by Mr. Dibyendu Bhattacharyya has been carried out under my guidance and this work has not been submitted elsewhere for a degree.

(Dr. S Bhargava)
Department of Materials and Metallurgical Engineering
Indian Institute of Technology,
Kanpur.

June 2005

ACKNOWLEDGEMENT

I would like to express my deep sense of gratitude to my advisor Dr. S. Bhargava for his expert guidance, support and encouragement throughout the present research. It was a great pleasure working with him.

I extend my special thanks to Mr. V. Kumar, Mr. Tripathi, Mr. Umashankar Singh, and Mr. Kartikayen for their necessary help during my experimental work. I would also like to thanks Mr.Verma for his help during compaction and rolling. I also wish to thank the entire all the staff of MME department and ASMS, who helped me at many occasions.

I would also like to thank sincerely my friends Pinaki Bhattacharyya, Anirban Chakraborty, Rajib Saha, and Debasis Chaira for not only their help and suggestions at various situations but also because they made my stay at IIT Kanpur a memorable one. Finally I would like the opportunity to thank all my lab mates Manoj Kumar, Anand Rao, Siddhiqui.

CONTENTS

			Pg
LIST OF FIGURES			vi
LIST OF TABLES			viii
CHAPTER 1		LITERATURE REVIEW	1
	1.1	Alloyed Ni Base Substrate Tapes With High Cube Texture Stability For Coated Superconductor Applications - A Review	1
		1.1.1 Introduction	1
		1.1.2 Pure Ni Substrate As A Substrate Material	3
		1.1.3 Alloyed Ni Base Substrates	9
		1.1.4 Alloyed Ni Tapes	12
		1.1.5 Solution Hardened Ni Tapes For Magnetic Applications	15
		1.1.6 Processing Route	21
		1.1.7 Conclusions	22
	1.2	Mechanical Milling	22
		1.2.1 Raw Materials	24
		1.2.2 Process Variables	24
		1.2.3 Mechanism Of Mechanical Milling	30
		1.2.4 Applications Of Mechanical Milling	34
	1.3	Nano Structured Materials	34
		1.3.1 Introduction	34
		1.3.2 Definitions And Classification Of Nano Structured Materials	35
		1.3.3 Structure Of Nanocrystalline Materials	38
		1.3.4 Consolidation Strategy For Nano Structured Materials	39
		1.3.5 Properties Of Nano Structured Materials	44

CHAPTER	2	EXPERIMENTAL PROCEDURE	46
	2.1	Starting Powder Characteristics	46
	2.2	Powder Milling	47
	2.3	X-Ray Diffraction	48
	2.4	Scanning Electron Microscopy	49
	2.5	Particle Size Analysis	49
	2.6	Powder Compaction	49
	2.7	Sintering Of Compacted Strips	50
	2.8	Cold Rolling Of Sintered Strips	50
	2.9	Estimation Of Density	51
	2.10	Optical Microscopy	51
	2.11	Hardness Testing	51
	2.12	Tensile Testing	52
	2.13	Fractography	52
CHAPTER	3	RESULTS AND DISCUSSIONS	53
	3.0	Introduction	53
	3.1	Characterization Of Mechanically Milled Powders	54
		3.1.1 Nickel-Tungsten Dispersion Or Mechanical Alloying	54
		3.1.2 Effect Of Milling Time On The Morphology Of Powder Particles	57
		3.1.3 Particle Size Refinement Of Ni-W Powders During Milling	59
		3.1.4 Reduction Of The Crystallite Size During Milling	60
	3.2	Sintering Of Strips	68
	3.3	Densification Rolling Of Sintered Strips	72
	3.4	Mechanical Properties Of Rolled Strips	77
		3.4.1 Microhardness Results	77
		3.4.2 Tensile Properties	77
	3.5	Fractography	79
CHAPTER	4	CONCLUSIONS	80

LIST OF FIGURES

		Pg
Fig 2.1	SEM Image of Starting W Powder	46
Fig 2.2	SEM Image of Starting Ni Powder	46
Fig 2.3(a)	Particle Size Distribution of Starting (Unmilled) Ni powder	47
Fig 2.3(b)	Particle Size Distribution of Starting (Unmilled) W powder	47
Fig 3.1	XRD pattern of Ni-30wt% W milled powders at different milling time	55
Fig 3.2	XRD pattern of Ni-10wt% W milled powders at different milling time	56
Fig 3.3	Comparison of the pattern of Ni-30wt% W powder milled 160hrs & Ni-10wt%W powder milled 60 hrs with that of pure Ni and W	57
Fig 3.4	Effect of milling time on crystallite size of Ni and W particles in Ni- 30 wt% W powder	62
Fig 3.5	Effect of milling time on crystallite size of Ni and W particles in Ni- 10 wt%W powder	62
Fig 3.6 & 3.7	SEM Image of Ni- 30 wt% W powder milled 5 hrs	62
Fig 3.8	SEM Image of Ni- 30 wt% W powder milled 15 hrs	63
Fig 3.9	SEM Image of Ni- 30 wt% W powder milled 25 hrs	63
Fig 3.10	SEM Image of Ni- 30 wt% W powder milled 40 hrs	63
Fig 3.11	SEM Image of Ni- 30 wt% W powder milled 60 hrs	63
Fig 3.12	SEM Image of Ni- 30 wt% W powder milled 80 hrs	63
Fig 3.13	SEM Image of Ni- 30 wt% W powder milled 100 hrs	63
Fig 3.14	SEM Image of Ni- 30 wt% W powder milled 120 hrs	64
Fig 3.15	SEM Image of Ni- 30 wt% W powder milled 160 hrs	64
Fig 3.16	SEM Image of Ni- 10 wt% W powder milled 25 hrs	64
Fig 3.17	SEM Image of Ni- 10 wt% W powder milled 40 hrs	64
Fig 3.18	SEM Image of Ni- 10 wt% W powder milled 60 hrs	64
Fig 3.19	EDS from W & Ni particles of Ni-30wt% W powder milled 40 hrs	65
Fig 3.20	EDS from W & Ni particles of Ni-30wt% W powder milled 100hrs	65
Fig 3.21	Particle size distribution of Ni-30wt% W powder at different	67

	milling times	
Fig 3.22	Particle size distribution of Ni-10wt% W powder at different milling times	68
Fig 3.23	Variation of density of single layered strips with composition	69
Fig 3.24	Variation of density of bilayered strips with milling time	69
Fig 3.25	Digital Images of Sintered Strips	71
Fig 3.26	Optical micrographs of a bilayered strip after first roll pass	74
Fig 3.27	Optical micrographs of a bilayered strip after second roll pass	75
Fig 3.28	Yield and tensile strength of different rolled strips	77
Fig 3.29	Engg. Stress-Strain Curve of Bilayered strip (Ni- Ni-10wt%W-milled 40 hrs)	77
Fig 3.30	Fracture Surfaces of Bilayered Strip (Ni- Ni-10wt% W milled 25 hrs)	79
Fig 3.31	Fracture Surfaces of Bilayered Strip (Ni- Ni-10wt% W milled 40 hrs)	79
Fig 3.32	Fracture Surfaces of single layered Strip (Ni- Ni-10wt% W milled 60 hrs)	79

LIST OF TABLES

		Pg
Table 3.1	Intensities, 2θ values and corresponding planes of tungsten collected from 2001 JCPDS	55
Table 3.2	Intensities, 2θ values and corresponding planes of nickel collected from 2001 JCPDS.	55
Table 3.3	Intensities and 2θ values of different peaks of Ni-30wt%W milled for 16 hrs	57
Table 3.4	Crystallite size of Ni & W in Ni-30wt%W milled powder at different milling times	61
Table 3.5	Crystallite size of Ni & W in Ni-10wt%W milled powder at different milling time	61
Table 3.6(a)	Density of sintered strips	68
Table 3.6(b)	Theoretical Density of strips	68
Table 3.7	Typical cold rolling & annealing cycle for densification of sintered strips	72
Table 3.8	Vickers Microhardness Values, HV (Kgf\mm^2) of Rolled Strips	76
Table 3.9	Tensile Properties parallel to the rolling direction	77

ABSTRACT

The milling behavior of nickel and tungsten powders, corresponding to Ni-10 wt% W and Ni- 30 wt% W compositions, during high energy milling in a planetary ball mill was studied. X-ray diffraction results obtained from powders milled up to 160 hrs show that both Ni and W remain in their elemental form without any mechanical alloying taking place between them. Morphological studies of milled powders show that both Ni and W powders become flaky and undergo fracture during high energy milling. W powder particles become finer and finer and get embedded in Ni forming an intimately mixed mixture. Single-layered Ni-10 wt% W and Ni-30 wt% W compacts made from milled Ni-W powders are well sintered at 900°C, i.e. at 0.68 T_M of Ni. Bi-layered Ni – Ni-W compacts made from the unmilled Ni powder and Ni-W milled powder develop a concave curvature towards Ni-W side due to enhanced sintering kinetics taking place in the Ni-W layer. The radius of curvature decreases as the milling time of the Ni-W powder increases. Sintered single- or bi-layered strips could be subjected to densification rolling by repeated cold rolling annealing cycles without facing any major difficulty. Thin bi-layered tapes of Ni – Ni-10 wt% W of thickness < 250 μm could be successfully prepared. Microhardness of sintered and rolled strips was measured. Mark improvement in microhardness values of the Ni base rolled single and bilayered tapes was observed when compared to that of pure Ni. Tensile tests on the finally rolled tapes showed yield strength ranging from 560 to 728 MPa and ultimate tensile strength ranging from 623 – 796 MPa. Both yield strength as well as the ultimate tensile strength of Ni – Ni-10 wt% W tapes increased with increasing the milling time. Analysis of the fracture surfaces of Ni – Ni-10 wt% W reveals the presence of fracture of predominantly the cleavage mode.

1.1 ALLOYED NI BASE SUBSTRATE TAPES WITH HIGH CUBE TEXTURE STABILITY FOR COATED SUPERCONDUCTOR APPLICATIONS - A REVIEW

1.1.1 INTRODUCTION

Ever since the discovery of high temperature superconductor in 1986, a world wide research endeavor has been directed towards developing long, flexible conductors with high critical current density (J_c) for a wide range of industrial applications. During the early periods in these efforts it was observed that randomly oriented polycrystalline HTS materials have critical current densities below 500 A/Cm^2. In contrast, oriented YBCO thin films grown epitaxially on single crystal oxide substrate such as (001) $SrTiO_3$ exhibit J_c values in excess of 1 MA/Cm^2 at 77K. This huge difference in critical current density values between randomly oriented HTS materials and single crystal like epitaxial film is attributed to the misorientation angle at the grain boundaries in polycrystalline materials. Value for J_c decreases significantly across the grain boundary as the misorientation angle increases with 'weak link' behavior observed for misorientation angle ~10°. So it can be well understood that to achieve a high J_c value the crystallographic orientation of the HTS wire or tape must have a high degree of grain alignment that is the conductor must have a pronounced crystallographic texture over its entire length.

One approach to producing a high-J_c HTS tape is to deposit a thick epitaxial film on a substrate material that has a high degree of in-plane and out-of-plane crystallographic texture and can be produced in long lengths. Epitaxial HTS films on single crystal oxides satisfy the requirements for high J_c, but it is not feasible to produce long lengths of these substrates. A very novel method to produce such substrate material has been developed at Oak Ridge National Laboratory, USA through thermomechanical processing where base metals such as Ni or Cu are rolled to high degree of deformation and recrystallized to obtain a very sharp, well developed cube texture on which epitaxial growth of buffer and YBCO film can be achieved . Such substrates which are biaxially textured and having chemically compatible surfaces for epitaxial growth of YBCO or other conductors have been referred to as rolling-assisted-biaxially-textured-substrates (RABiTS™). A schematic diagram of the RABiTS™ process has been shown in Fig 1.1. Current densities above

10^6 A/cm^2 have been reported in case of YBCO coated on such substrates. The first metals used for biaxial texturing for superconductive applications were Ag and Ni. But silver is technically not attractive due to its lack of strength, cost and inability of developing a sharp cube texture. Amongst the metallic elements Ni has been widely used as a substrate material because of good oxidation resistance and the good lattice mismatch with $YBa_2Cu_3O_7$. However, the YBCO can not be directly deposited on Ni substrate because of the chemical reaction between Ni and YBCO at high temperature. To suppress the Ni diffusion into YBCO, A-(001) oriented oxide buffer layer epitaxially grown serves two purposes. The buffer layer maintains the sharp crystallographic texture of the substrate material and acts as a thermal diffusion barrier preventing the diffusion of substrate material into the HTS material and chemical reaction with the substrate material. The primary objective to develop a substrate material is to develop a strong cube texture which assures texture stability at the deposition temperature. But in addition there are several other criterions like the strength of the substrate which is very essential in actual fabrication time. To improve the strength of the Ni substrate it is essential to introduce alloying elements to pure Ni which has a very low tensile strength. For this reason there has been a progressive shift towards developing an alloyed Ni base substrate rather than pure Ni. It remains the challenge to identify the specific alloying elements and alloy content for specific requirements.

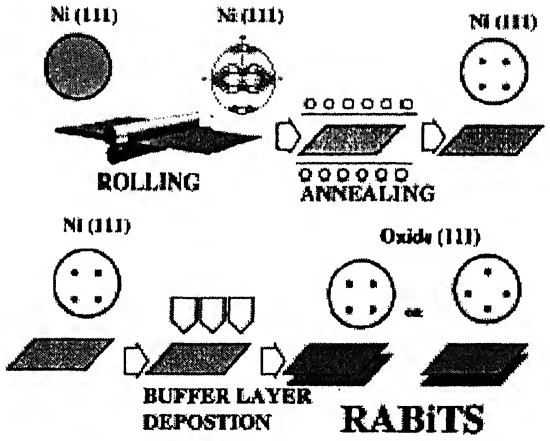

Fig. 1.1: Fig. 1: Schematic representation of the RABiTS process. Starting with a randomly oriented Ni bar/plate, cold-rolling is used to produce a distinct Cu type rolling texture. This is followed by recrystallization to a cube texture. Epitaxial material/oxide buffer layers are then deposited on the textured surfaces [A. Goyal, S.X. Ren, E.D. Specht, D.M. Kroeger, R. Feenstra, D. Norton, M. Paranthaman, D.F. Lee and D.K. Christen, "Texture formation and grain boundary networks in rolling assisted biaxially textured substrates and in epitaxial YBCO films on such substrates", *Micron*, Vol. 30, 1999, pp. 463-478].

1.1.2 PURE NI SUBSTRATE AS A SUBSTRATE MATERIAL.

Rolling and annealing of fcc metals such as Cu, Ni and Al leads to {100} <100> or 'cube texture' as defined in Fig.1.2. This cube component is important due to several reasons. Firstly, this cube component is very sharp; it is mostly a single component texture i.e. it develops with a large fraction of the grains near the ideal cube orientation with little misorientation among them. In addition Ni is a relatively high m.p. metal and is resistant to high temperature oxidation. This helps in the epitaxial growth of the YBCO film with an intermediate buffer layer.

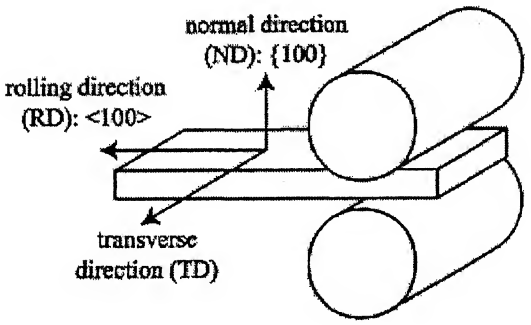

Fig.1.2. Definition of the notation for cube rolling texture

Cube texture in Ni can be formed after heavy cold rolling and subsequent annealing as the primary recrystallization texture. The intensity of cube texture in Ni has been found to depend on a no. of factors amongst which the purity of Ni is most important. Presence of impurity even in ppm level can adversely affect the recrystallization behavior and consequent texture development. The most detrimental effect has been found to be the presence of sulfur. It significantly affects the recrystallization characteristics of Ni. Eickemeyer *et al.* have shown that the purity of Ni have significant bearing on the sharpness of the cube texture. They measured the intensity of the cube component after cold rolling and annealing of two grades of Ni powder with 99.98% and 99.94% purity. The relative intensity of the cube component was found to be significantly higher in case of the Ni powder with greater purity as evident from Fig. 1.3. The less pure Ni (99.94%) was found to be more prone to secondary recrystallization.

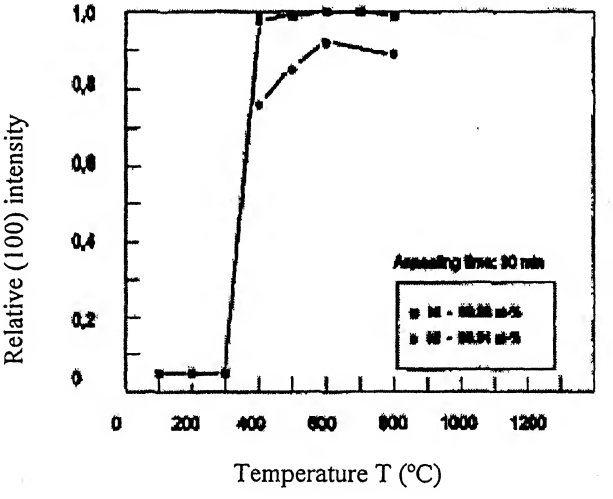

Fig. 1.3: Effect of Ni purity on intensity of cube texture

Goyal *et al.* first in detail studied the possibility of using pure Ni as a substrate material. They cold rolled pure Ni to more than 90% deformation followed by recrystallization annealing at 1000C for 4hrs. A very sharp, well developed, single component cube texture was reported. The full width half maximum (FWHM) value with x-ray ω and φ- scan was reported as 6^0 and 7^0 respectively. Investigation on the misorientation angle in millimeter size regions of the substrate with over 100 interconnected grain boundaries yielded that over 95% of the grain boundaries had misorientation angle less than 10^0 i.e. there were very few high angle grain boundaries and most of the grain boundaries were low angle grain boundaries. The grain size was in the range of 50-100μm and controlled roll surface lead to a very smooth as rolled

substrate with fairly small surface roughness 10 nm which is very essential for epitaxial film growth. The subsequent deposition of YBCO with different combination of buffer layer yielded critical current densities exceeding 10^5 A/Cm^2 in certain buffer configuration.

Specht *etal.* studied the optimum rolling and annealing condition for such Ni substrate. They conducted investigation on pure Ni over a range of annealing temperature (300-1375^{0}C). They reported that at 300^{0}C annealing temperature the primary recrystallization texture consisted of 94% cube component ({100} <100>) and 6% twin component ({221} <221>). But with higher annealing temperature and time the twin component gradually disappears and practically no twin component is observed above for annealing at 1200^{0}C. But higher temperature leads to increased surface roughness. According to them a thickness of 125μm leads to an optimum texture.

The strengthening of the cube component at higher annealing temperature has been also reported by other investigators. Zhou *et al.* reported that for an ultra pure Ni sample (99.999%) and for commercially pure Ni sample (99.95%) strong cube component are present in both the samples at 1200^{0}C annealing temperature. For 99.999% Ni sample the sharpness of the cube component increases with an annealing process using a continuous heating ramp up to 1200^{0}C.

But pure Ni has also some major disadvantages to be used as a substrate material. In the deposition temperature range, in which buffer and YBCO films are deposited on the substrate (~ 700-900C), abnormal grain growth or secondary recrystallization i.e. a preferential growth of minor texture component consuming major texture component can take place which may destroy the cube texture altogether. De Boer *et al.* reported with the aid of EBSP studies the influence of grain growth on texture Ni tapes annealed at two different temperatures, namely, 550^{0}C and 600^{0}C as shown in Fig.1.4. They found that after moderate grain growth characterized by slow growth of cube textured grains, some grains start to grow very fast as depicted in Fig. 1.4(a) and 4(b). This abnormal grain growth becomes very prominent at 600^{0}C. After further annealing the cube texture was found to be destroyed altogether since the grains which grow to size of about 1mm are randomly oriented as in Fig. 1.5. Markita *et al.* using lower purity Ni (99.95% vs. 99.99%) reported that secondary recrystallization occurs once the grain size reaches the final value. Contrary to the above findings Specht *et al* reported that no secondary

recrystallization occurs even at 1375^{0}C even when the final grain size is reached at 600^{0}C.

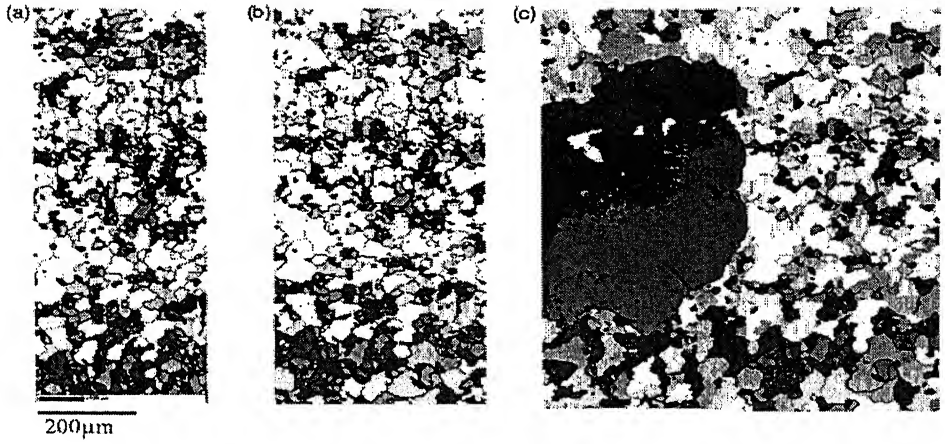

Fig 1.4. Anomalous grain growth (secondary recrystallization) in Ni. EBSP-mappings of a sample annealed successively at increasing temperatures: (a) 500°C/30 min, (b) 550°C/30 min and (c) 600°C/30 min. Dark grains are highly misoriented with respect to the exact cube orientation. Grain boundaries with misorientations between 5° and 10° are marked by a gray line, grain boundaries with misorientation angles above 10° by a fat black line in the EBSP-maps

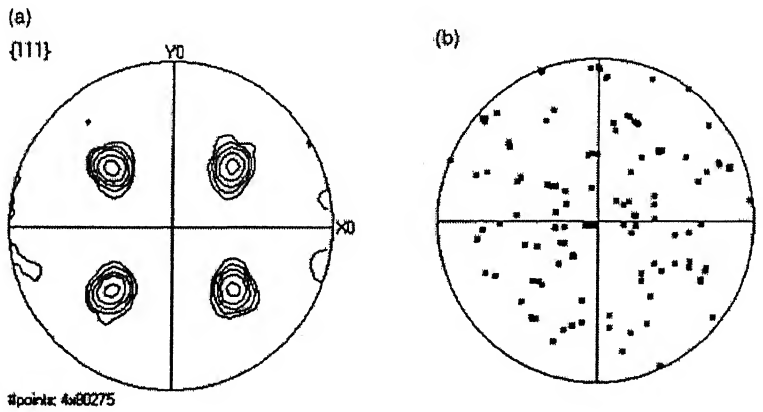

Fig.1.5. {111}-pole figures determined with EBSP of (a) the as recrystallized Ni Sample annealed at 500°C/30 min and (b) the orientations of giant grains grown due to abnormal grain growth

A necessary condition for abnormal grain growth is the existence of highly mobile high angle grain boundaries. Due to this those grains which are highly misoriented towards the surrounding cube grains can only grow, The mobility of grain boundaries depends upon the impurities either present as solute or secondary phase particles other than the misorientation angle. Solutes which are segregated at the grain boundaries interact with the grain boundaries so that the migrating grain boundaries have to drag the solute with it reducing the grain boundary mobility. It is well known that finely precipitated secondary phase particles have a pinning effect on the grain boundaries because the free energy is reduced if the grain boundary and phase boundary coincide. This is the so-called Zener drag.

Abnormal grain growth may take place if somehow the mobility of the grain boundary is enhanced. This may take place in case of solute drag effect where with increasing temperature the solubility is increased and the segregated solute is taken into solution and thus the grain boundary segregation becomes considerably less. In case of Zener drag the grain boundary mobility may increase. Here grain boundary mobility may increase due to the phenomenon of Ostwald ripening. The pinning force may decrease because the particle distance becomes larger. In both the mechanism some boundaries may become mobile earlier than the others leading to the preferential growth of only few grains.

In addition to the secondary recrystallization or abnormal grain growth another concern is the grain boundary grooving at high annealing temperature. Due to this phenomenon, atoms at the grain boundaries meeting the surface of the tape diffuse along the surface or through the bulk out of the grain boundary region and thus causes a ditch at the surface and an enrichment of the material on both sides of the ditch as shown in Fig. 1.6. Groove formation may occur by an evaporation condensation mechanism or surface diffusion process with the groove profile depending up on formation mechanism, the processing conditions, annealing temperature and time, grain boundary energy, the surface energy and the diffusion coefficients of the grain boundary and the surface. Amongst these the processing condition, annealing temperature and time are found to have most important contribution. Gladstone *et al* conducted AFM and EBSD studies on the grooving phenomenon in cube textured Ni tapes. They reported that there is a significant correlation between the groove depth and the misorientation angle at the grain boundaries. The depths of the groove at low angle grain boundaries are rather low as compared to the high angle boundaries and

the Σ3 or the coincident lattice site boundaries showing a wide average range of groove depth. The typical values for low angle grain boundary grooves are 300Å and some high angle grain boundaries have depth greater than 1200Å. The grain boundary groove depth was found to be dependant up on the annealing atmosphere with Ni annealed at Ar-4% H_2 atmosphere showing lower average groove depth than Ni annealed at vacuum. The dependencies of groove depth on misorientation angle and annealing atmosphere can be appreciated from Fig. 1.7.

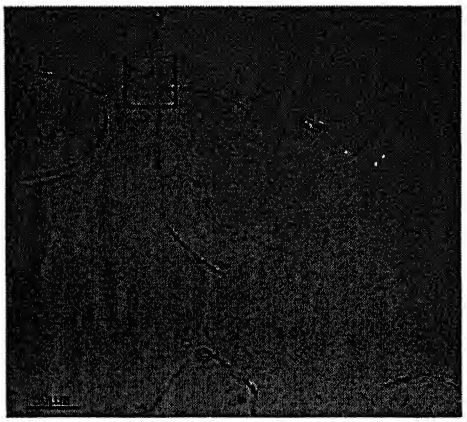

Fig 1.6. Optical micrograph of a cube texture Ni tape showing thermal etching at the grain boundaries

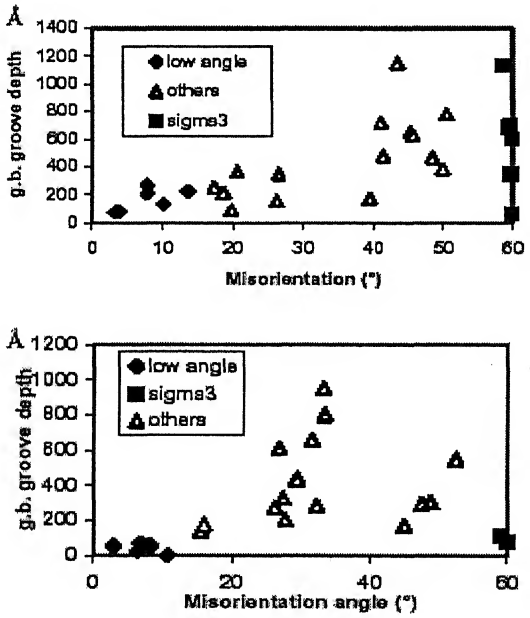

Fig.17. (a) Graph showing the relationship between the grain boundary groove depth and the misorientation for Ni tape recrystallized in vacuum at 800^{0}C for 4h and (b) recrystallized in Ar-1%H_2 at 800^{0}C for 4h

Pure Ni has low tensile strength typically about 550MPa in annealed condition which limits the possibility of producing and coating very thin tapes, typically in the range of 20-30 μm that is necessary to achieve a high engineering current density. Also Ni is ferromagnetic with a curie temperature of 627K. So at the liquid nitrogen temperature (77K) Ni is sufficiently ferromagnetic. In alternating current applications this may lead to a significant energy loss due to hysteretic loss in the magnetic material.

As now it can be clearly understood that pure Ni has some inherent problem associated with it, it was felt necessary to design such substrate materials which will be strong enough and also suitable for alternating current application. The classical metallurgical approach to the above problem is solid-solution strengthening of pure Ni through alloying elements addition. There have been tremendous research thrust in recent years to develop strong as well as non-magnetic Ni base substrates which can retain their cube texture at the deposition temperature. A number of metallurgical systems have so far been identified based on Ni which seems potentially suitable to meet those requirements.

1.1.3. ALLOYED NI BASE SUBSTRATES

There are certain alloy design issues which are to be addresses while developing a suitable Ni based substrate. Amongst them most important are:

- Development of Texture in Ni alloys
- Selection and content of alloying element for specific application

It has long been established that the addition of alloying element to Ni reduces the stacking fault energy (SFE) which influences the rolling texture and subsequently the recrystallization texture. In fact high alloying addition may completely suppress the cube component. So it is of prime importance to ensure that solution hardening due to alloying addition should not interfere with the formation of a sharp cube component in the recrystallized material.

1.1.3.1 SELECTION AND LEVEL OF ALLOYING ELEMENTS

From the above discussion it should be clear that the alloying element must conform to the following conditions:

- The stability of the cube texture in Ni is very prone to the presence of the alloying elements. So the alloying element must not adversely affect the recrystallization and texture formation.
- Since the tapes to be used should in a very thin substrate form (~20-30 μm) therefore they should be sufficiently strong. Also since the long tapes are to be pulled through a processing chamber at deposition temperature of 700-800C strength factor is very important. Therefore, the alloying elements should increase the material strength.
- As in the deposition temperature range abnormal grain growth takes place leading to the destruction of the cube texture in Ni. Texture stability must be guaranteed at coating temperature usually in the range of 700-800^0 C. A necessary condition for abnormal grain growth is the existence of high angle grain boundary. For this reason, only grains which are misoriented towards the cube grains are able to grow, since only these grains have and keep high misorientations during their growth into the environment of mostly cube oriented grains.
- The alloying elements should suppress the undesirable impurity actions and, possibly, result in increased cube texture sharpness and a high thermal stability against secondary recrystallization at the processing temperature.

1.1.3.2 POTENTIAL NI BASED ALLOY SYSTEMS TO BE USED AS THE SUBSTRATE MATERIAL

The suitable alloying elements to meet the above mentioned criterion are elements of group VA and group VIA of the periodic table as identified in Fig. 1.8. The reasons behind the selections of these elements are:

- All these elements are high melting point metals i.e. so called refractory metals. Due to their high melting points they are able to increase the primary recrystallization temperature in Ni. Table 1.1 gives an idea of the melting point of these metals in comparison to pure Ni.
- These elements are able to strengthen the grain boundaries in nickel even when present in a micro-alloying level (≤2000 wt ppm).
- The chemical affinity of these elements particularly Mo or Ta towards deleterious impurities, namely sulfur, is stronger than that of Ni. So they can

form sulphides and suppress the detrimental effect of sulfur on recrystallization texture.

- There exists significant solid solubility of these metals in Ni which is helpful in solid-solution strengthening and increase the tensile strength of the derived tape.
- The metals particularly Cr, V and Mo can suppress the ferromagnetic property of Ni beyond 77K when added in larger quantities .

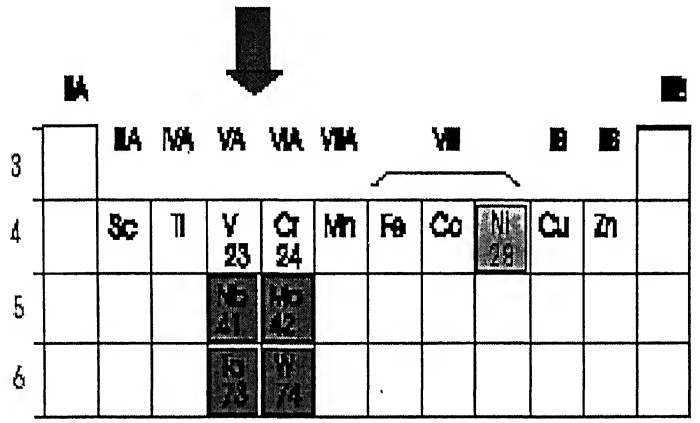

Fig.1.8. Elements belonging to fourth period of periodic tables

Table 1.1: Comparison of Melting points of various refractory element

Element	Melting point Ratio with Ni ($T_{m, Ni}/T_{m, R}$)
Vanadium	0.791
Chromium	0.792
Niobium	0.628
Molybdenum	0.596
Tantalum	0.525
Tungsten	0.467

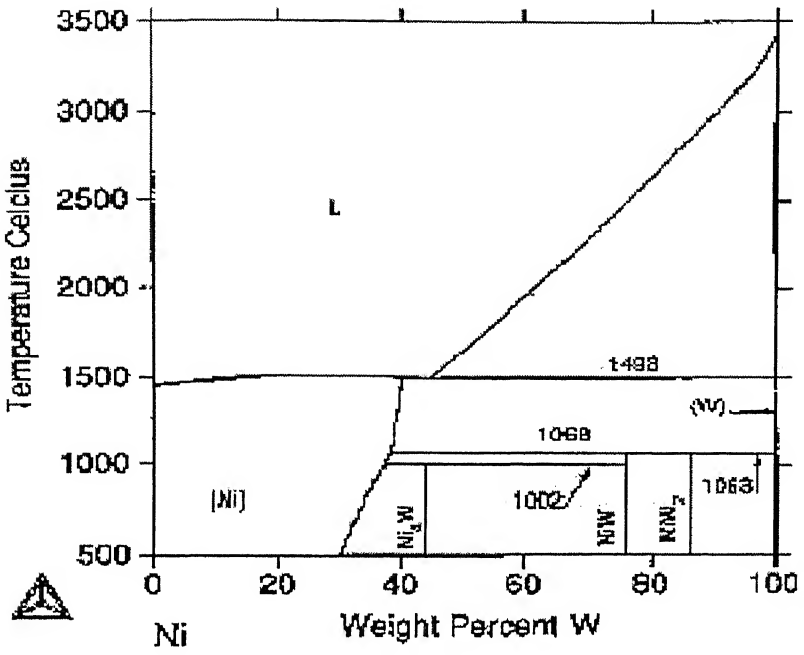

Fig 1.9 Ni-W Phase Diagram

1.1.4. ALLOYED Ni TAPES

1.1.4.1 EFFECT OF MICRO-ALLOYING ON TEXTURE FORMATION AND TEXTURE STABILITY

The beneficial effects of micro-alloying Ni with refractory metals on development and stability of texture have been reported by many investigators. Eickemeter *et al* studied the influence of small addition (~0.1%) of Mo, W, Nb and Ta with Ni in both low and high temperature annealing region. They reported that in comparison to pure Ni (99.94 at %) the micro alloying yielded an increased (100) X-ray reflection intensity after annealing up to 1100^0C as shown in Fig.1.9. The evaluation of the pole figures and EBSD mappings of the Ni-0.1 at% W and Ni-0.1 at% Mo material revealed a strong cube texture. The measured intensities of the nickel with 0.1 at% tantalum were 1.0 over the annealing temperature range of 800-1100^0C and after annealing at 850^0C the micro-alloyed Ni tapes with 0.1 at% niobium also offered the maximum relative intensity value of 1.0 with FWHM values between 6.7 and 7.5^0. Consequently, the four refractory metals were very effective in micro-alloying the 99.94 at% nickel in order to enhance the temperature region in which the recrystallization cube texture behaves considerably more stable

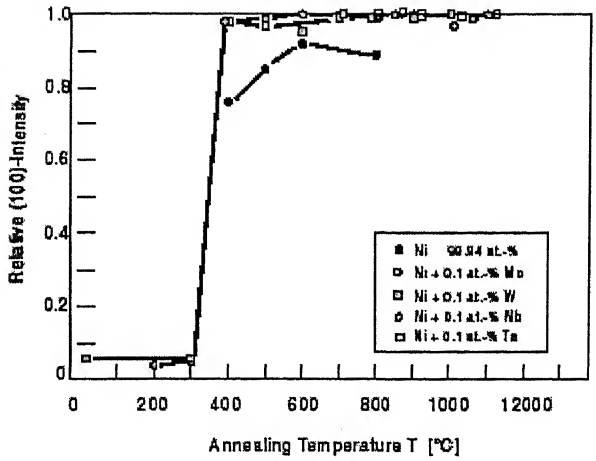

Fig.1.10 Influence of micro-alloying of Ni with Mo, W, Nb and Ta on the relative (100) x-ray reflection intensity after annealing at defferent temperatures over 30 minutes

Goyal *et al.* studied the influence of minor addition of W and Fe, 3at. % and 1.7 at% respectively, to Ni in a under different conditions of temperature and time. For lower annealing temperature they reported a significant amount of retained texture present in the material. For annealing temperatures of 1200^0C and in flowing Ar-4%H_2 atmosphere they found the substrate completely textured. Upon annealing at 1400^0C, the texture sharpened considerably. The grain boundary misorientation distribution (GBMD) with the help of EBKP studies proved that the most of the grain boundaries were low-angle type which is essentially required to accomplish a high *Jc* value. High critical current densities, up to 1.9 MA/Cm^2 at 77K, self-field were demonstrated on this substrate using a multilayer configuration YBCO/CeO_2/YSZ/Y_2O_3/Ni-3at%W-1.7at%Fe.

Varesi *et al* studied the texture development in three Ni alloys, namely, Ni-11at. % V, Ni-13%Cr and Ni-5at. % W. They reported that Ni-V and Ni-Cr substrate have a greater concentration of twinned cube textured and misoriented grains in comparison to Ni-5at.% W. From optical microscopic analysis they determined the volume fraction of twinned cube textured grains for Ni-11at. % V, Ni-13%Cr and Ni-5at. % W which turned out to be 0.17, 0.15 and 0.05. The ratio of the area representing the cube oriented grains with respect to the substrate area was found to be 0.96, 0.97 and 0.99.

Eickmeyer *et al* investigated the microstructural conditions particularly the initial grain size effect for the achievement of a perfect annealing cube texture in Ni-5at%W alloy. Starting with two Ni-5at% W alloys with different grain size, they reported that the resulting cube texture was rather well developed and strong in the material with lower grain size. Subsequent coating of the stationary tape with CeO_2 buffer and superconducting YBCO layers resulted in critical current densities up to .2 MA/Cm at 77K and zero fields on tapes of 20 cm in length.

As it was pointed out earlier that abnormal grain growth or secondary recrystallization and existence of deep thermal grooves can substantially interfere with the epitaxial growth of the buffer layers on the substrate, therefore the suppression of the grain boundary grooving would appreciably improve the conditions during subsequent layer deposition.

1.1.4.2 EFFECT ON SUBSTRATE STRENGTH

Since the superconductor coating does not withstand a strain above 0.5% in compression and 0.2% in tension without degradation, the stress at low strains (e.g. 0.2% yield strength) is more critical for applications as a substrate material . Goyal *et al.* reported that Ni substrate with minor alloying additions of W and Fe is significantly stronger than the 99.99% Ni substrate. The average yield strength of Ni-3at.%W-1.7at.%Fe at .02% and 0.2% strain increases to 143MPa and 154MPa as compared to 99.99% pure Ni sample which is only 40 and 58MPa at the same strain level. The improvement in tensile strength has been reported for Ni-5at.%W by Rupich *et al* [22]. The tensile strength of Ni-5at.%W was found to be 178MPa at room temperature. At the operating temperature of 76K for these substrate materials the tensile yield strength of Ni-5at.%W is more than four times higher than that for pure Ni whereas the Young's modulus and proportional limit are higher by a factor of 1.8 and 2.25 respectively where as the strain-hardening of pure Ni was found to be as shown in Fig. 1.10 . Improvement of mechanical strength due to micro alloying is believed mostly due to solid solution hardening. A strength increase because of solution hardening in Ni depends on the specific alloying elements via their diameter mismatch with Ni. The relatively larger solute atom diameters of Mo (+11%), W (+12%), Nb(+16%) and Ta (+17%) should lead to a stronger effect than the elements of the fourth period, such as Cr (+2%) and V (+7%) . But the strength of Ni-refractory metal tapes at the processing temperature has not been reported in literature so far.

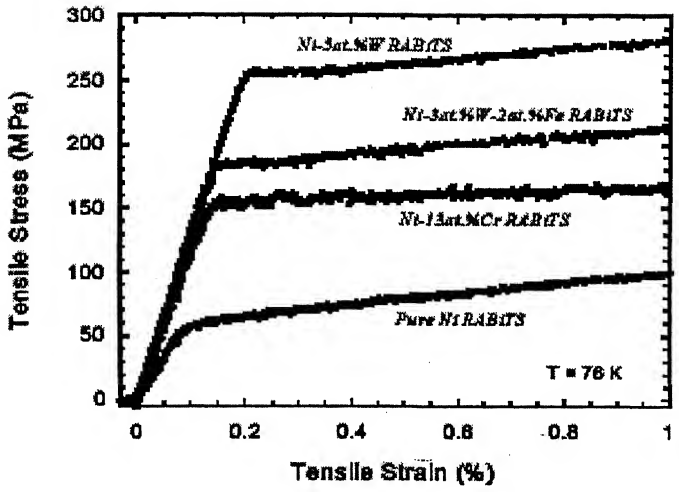

Fig.1.10 (b). Comparison of stress-strain curves at 76K of pure Ni, Ni-13at.% Cr, Ni-3at.% W-2 at.% Fe and Ni-5at.%W alloy RABiTS tape

1.1.5. SOLUTION HARDENED NI TAPES FOR MAGNETIC APPLICATIONS

1.1.5.1 SELECTION OF ALLOYING ELEMENTS FOR SUPPRESSING THE CURRIE TEMPERATURE

An obvious consideration for using Ni as a substrate material is that Ni is ferromagnetic with a curie temperature of 627K and a saturation magnetization of 57.5 emu/g . So it can be easily understood that Ni is ferromagnetic at the liquid N_2 temperature of 77K. The ferromagnetism of Ni adds to the complexity of design of the high field magnets. In addition to this the use of Ni in alternating current applications may lead to increased energy losses due to hysterisis loss in the substrate material. The actual energy loss per cycle of applied magnetic field H is given by the area enclosed within a magnetization loop M(H), and this varies with the magnetic "hardness" of the ferromagnet. Keeping these considerations in view it is obviously desirable to develop suitable alloys with reduced ferromagnetism which can be successfully biaxially textured.

The potential alloying elements to reduce ferromagnetism of pure Ni are Cr, V, Si, Al and Ti as can be seen from Fig.1.11 though the solubility of Ti, Al and Si are not high enough to suppress the Curie temperature below 77K . But Cr and V are mostly preferred as alloying elements for such applications as only Ni-Cr and Ni-V

alloys are found to develop a strong cube texture against the general tendency that with higher alloying content the cube texture intensity goes down drastically.

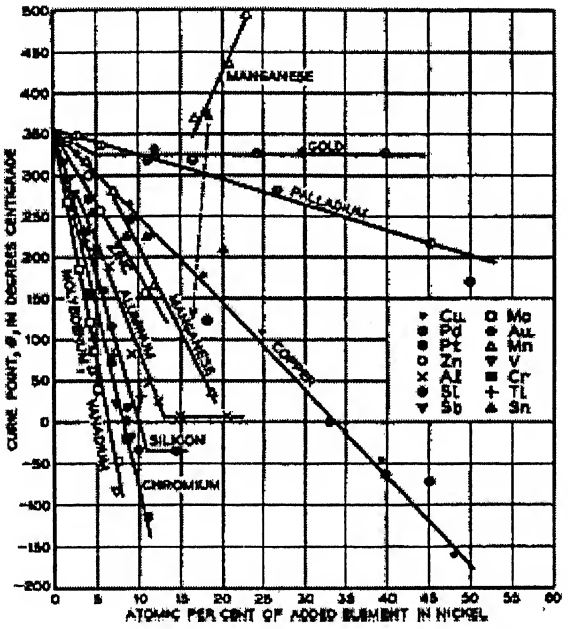

Fig.1.11. Dependence of the Curie temperature on the alloying elements

Thompson *et al.* studied a series of Ni-Cr alloys with increasing Cr content up to 13% for that purpose. They reported that mass magnetization M(T) decreases steadily along with the curie temperature (T_c) with increasing Cr content as can be seen from Fig. 1.12 . The reported values hysterisis energy loss/cycle of the Ni-7%Cr alloy were 1400 erg/cm^3 and 2000 erg/cm^3 with a coercive field of 4 Oe at 77K with the applied magnetic field parallel to the plane of the foil and parallel to the normal of the plane of the foil respectively (Fig. 1.13a)). In contrast the hysterisis loss/cycle of the pure biaxially textured Ni was found to be 18, 200 erg/cm^3 with the field parallel to the normal to the plane of the foil and a coercive field of 7 Oe (Fig.1.13b)). For coated conductor applications materials will be used at large magnetic fields or to generate such magnetic fields. Therefore the field dependent magnetization is a very important consideration. Ni-Cr alloys with lower Cr content, typically with 7 and 9 at% are found to be ferromagnetic, whereas Ni-11at.%Cr alloy are found to be paramagnetic with significantly lower magnetization which is comparable to annealed 304 type stainless steel and Ni-13at.% Cr alloy with even lower magnetization at the temperature of 40K and 77K as can be seen from Fig. 1.14

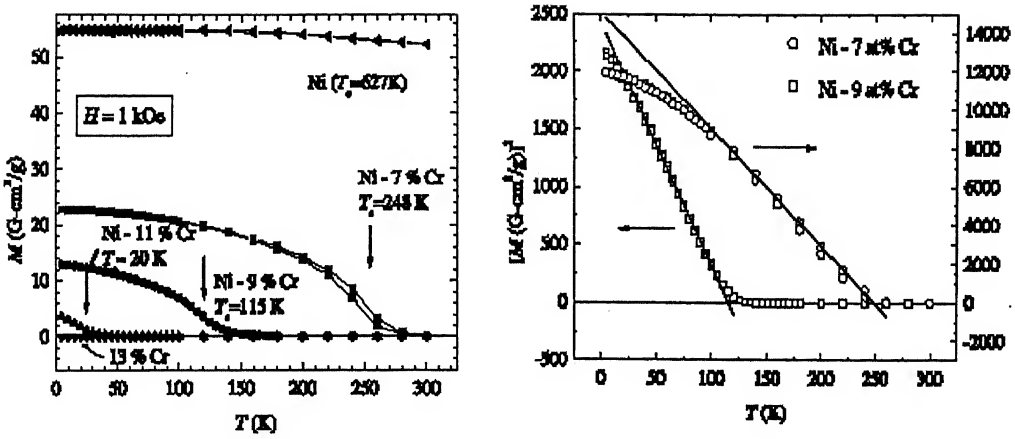

Fig 1.12. a)The Mass magnetization of Ni-Cr alloys vs. temperature measured in an applied magnetic field H=1 KOe applied parrallel to the plane of the foils. Nominal Cr concentration is given in at % and b) A plot of M^3 vs. temperature T. Straight lines show the extrapolation to M=0 used to define the curie temperature

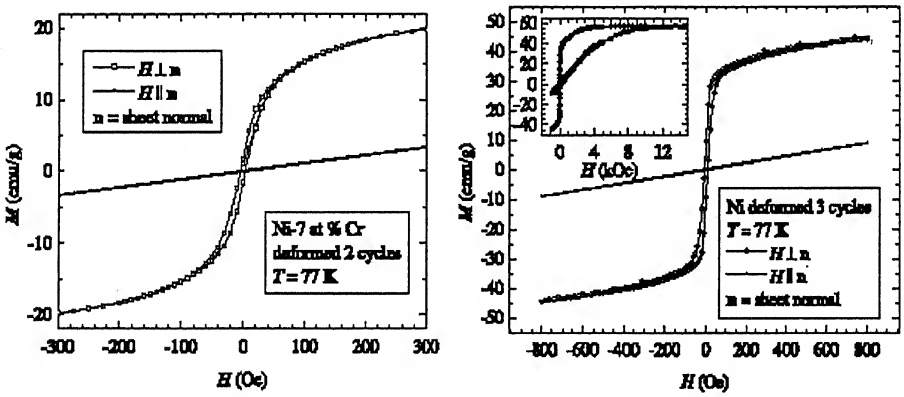

Fig 1.13 a) Magnetization loops (expanded scale) for a deformed Ni93Cr7 foil at 77 K, with magnetic field applied parallel or perpendicular to the plane of the foil. The magnetization is relatively reversible, with limited hysteretic energy loss/cycle and b) Magnetization loops for a deformed biaxially textured Ni foil at 77K, with magnetic field applied parallel or perpendicular to the plane of the foil inset: magnetization in large fields

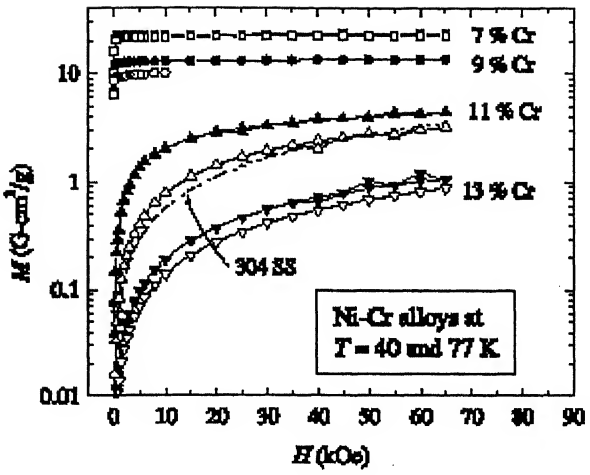

Fig. 1.14 The field dependence of the magnetization of different Ni-Cr alloys

1.1.5.2 DEVELOPMENT OF TEXTURE

The basic requirement for substrate materials for coated conductor is development of a strong cube texture as has been pointed out earlier. Since the alloying element content for non magnetic substrate is generally on the higher side it is therefore important to ensure that the higher alloying addition does not impair the cube texture of the substrate material. De boer *et al.* studied the several Ni based systems to determine the preferred alloying elements which can develop a sharp cube texture at higher alloying addition. According to their studies non-magnetic alloys in which cube texture component is found after recrystallization are Ni-13at.%Cr, Ni-9at.%V and Ni-55at.%Cu alloys (Fig. 1.15). Sharp cube texture component was reported by De boer *et al.* for Ni-13at.%Cr and Ni-9at.%V recrystallized at 900C which was confirmed by misorientation distribution determined with the aid of EBSP studies (Fig. 1.16). The intensity of the cube texture improves with increasing annealing temperature until the onset of abnormal grain growth which was found to be temperatures exceeding 950C (Fig. 1.16b). Thompson *et al* reported that Ni-Cr alloys can be thermo-mechanically processed to develop a very strong cube texture component up to a Cr content of 13 at.% Cr. (111) X-ray pole figure of a Ni-13at.% Cr annealed at 1050°C for 2hrs. has been given in Fig 19. It can be noted that only four crystallographically equivalent peaks corresponding to the {100}<100> cube

orientation are present in the pole figure quantification of which revealed presence of ~100% cube orientation.

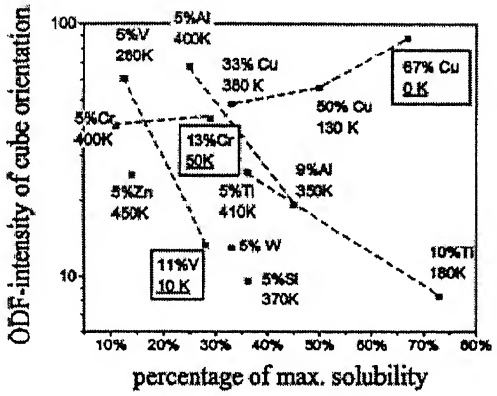

ig. 1.15. Dependence of cube intensity of several Ni-alloys on the alloying content scaled to the to the absolute maximum solubility. The legends on the data point stands for the absolute content in at.% and the estimated Curie temperature

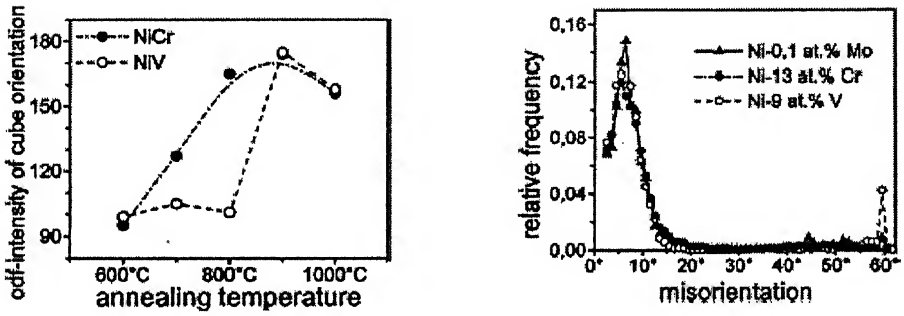

Fig. 1.16. (a) Texture development of the alloys Ni-9at%V and Ni-13%Cr with annealing temperature and (b) misorientation distribution of different Ni alloys

But the main difficulty of using Cr or V as the alloying elements to Ni is that both these elements are very prone to oxide formation and this becomes much easier at the buffer/YBCO deposition temperature around 700-800°C. The formation of Cr/V

oxide is detrimental for the epitaxial growth of the buffer and YBCO layer. Hence, it must be understood that oxidation resistance is a critical property for a metallic substrate. Components of Ni alloys have different affinities for oxygen and are also strongly affected by oxidizing conditions, surface finish, grain size, sample thickness, size and alloy composition. Often the simple kinetic rate equation for oxygen diffusion is not followed and the scale changes in a very complex way . Tuissi *et al.* studied the oxidation rate of Ni-Cr-W and Ni-Cr-V alloys by thermogravimetric analysis [Fig. 1.17].

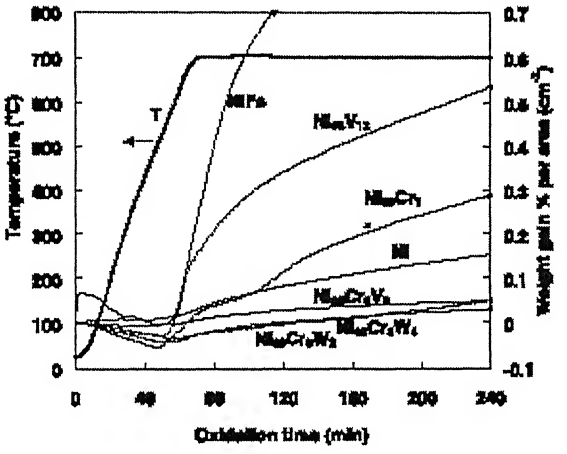

Fig.1.17. Oxidation behavior of pure Ni and different Ni base alloys

As compared to the binary alloys of Ni-Cr, Ni-V the ternary alloy system Ni-Cr-W and Ni-Cr-V showed substantially lower weight gain less than .03% g/cm^2. It may be noted from the figure that pure Ni shows better oxidation resistance than both Ni-Cr and Ni-V alloys. The weight gain for Ni-Cr sample was attributed mainly due to the uncompleted formation of protective Cr_2O_3 layer. Optical Microscopy of Ni-Cr-W and Ni-Cr-V revealed more uniform scale formation in case Ni-Cr-W alloys as compared to Ni-Cr-V alloys. Both Ni-Cr and Ni-V alloy systems shows non uniform oxidation principally at the grain boundaries where Cr_2O_3 grows . It appears that addition of W improves the oxidation resistance of Ni-Cr alloys.

Another recent approach is the formation textured NiO on the surface of Ni-Cr alloys through surface oxidation epitaxy . Very recently Lockman *et al.* have reported in detail the oxidation behavior of Ni-10at.%Cr and Ni-13at.%Cr. They found that air oxidation of Ni-Cr foils at 1050C can produce a smooth, highly textured NiO surface

oxide which can efficiently act as a first buffer layer in a superconducting coated architecture.

Sharma *et al.* suggested a functionally graded composite substrate material Ni–3%W/Ni–10%Cr–1.5%Al to overcome the surface oxidation problem. Ni-5at.%W alloy was used as the outer layer since Ni-W alloys develop strong cube texture upto 5at.%W and Ni-W alloys have good oxidation resistance whereas Ni-10at.%Cr-1.5at.%Al was used as the inner core as Cr can suppress the ferromagnetism beyond 77K as discussed earlier. The inner core and outer layer was so chosen that the strength level does not differ too much to prevent inhomogeneous deformation which may lead to cracking. Al was used in the substrate material to precipitate Al_2O_3 by controlled internal oxidation to increase the strength level further. The substrate was reported to develop strong cube texture determined with EBSD studies at the surface when annealed at 950C after cold deformation. Majority of the grain boundaries were reported to have misorientation angle less than 10° with maximum in the misorientation distribution close to 7° (low-angle grain boundaries) . The composite showed reasonably good tensile propertied with yield strength exceeding a factor of four when compared to pure Ni and substantially more than that of Ni-10%Cr-1.5%Al. There was conformity in the strength level of the inner core and the outer core Thus functionally graded composite materials appears to be a technologically very attractive solution though it demands further and dedicated effort at its current level of development.

1.1.6. PROCESSING ROUTE

The proper processing route of these substrates is one of the major issues as far as the practical application is concerned. So far the substrates have been prepared by both conventional melting and casting route and standard powder metallurgical techniques. But there have been no studies available to establish the supremacy of one process over the other. But it might appear to be quite reasonable that since the purity of Ni is one of the most important issues for developing a strong cube component so powder metallurgy techniques are better from that perspective as melting route may inadvertently introduce some deleterious impurities. Though it has been reported in literature that substrates prepared through melting and casting route develops sharp cube texture after cold deformation and annealing but at the same time necessity of strict quality control during the whole procedure can not be ruled out. In addition, the

initial grain size can be better controlled in P/M technique by using very fine powder and the processing temperature is much lower than that of melting techniques.

In powder metallurgy techniques also substrates have been prepared through the normal practice of starting from a very fine and pure Ni powder and subsequently pressing them to green compact followed by sintering of the compact. Recently Lee *et al*] has investigated the possibility of employing cold-isostatic pressing (CIP) followed by sintering and cold rolling for preparing the initial substrate. The substrate was subjected to X-ray studies with encouraging result of sharp cube texture intensity developed after annealing at 1000^0C. An alternative to the RABiTs method of cold-rolling and annealing based upon electrodeposition process under applied magnetic field has very recently been reported and under investigation for further development

1.1.7. CONCLUSIONS

Biaxially textured Ni base alloys prepared through RABiTS method have been established as techno-economically viable solution for using as substrate material for coated super conductor applications. But proper alloy design is the key issue to their successful applications. The properties of these alloy substrates are to be tailored in such a way that these substrates develop very sharp cube texture component after recrystallization with good texture stability at high temperature. At its current state of development most potential alloying elements are W and Mo at the micro alloying level and Cr at higher quantity for non magnetic applications requiring a very low hysterisis loss. Another technologically and viable means is preparing Ni base functionally graded composite materials, but further research is necessary to establish their supremacy.

1.2 MECHANICAL MILLING

Mechanical milling of powders using high energy ball mill has proved itself to be the most powerful method for the production of nanostructured materials because of its simplicity, relatively inexpensive equipment ,and the possibility of producing large quantities, that can be scaled up to several tons. Mechanically processed micron sized powders have been shown to posses nanosized substructures or even to become amorphous with appropriate milling parameters. In most systems, the nano grains or

amorphous structure represents a far from equilibrium condition that is generally quite metastable in nature.

Mechanical milling is normally a dry, high energy milling technique and has been employed to produce a variety of commercially useful and scientifically interesting materials. This technique was developed around 1966 by john S. Benjamin and his colleagues at the Paul D. Merica Research laboratory of the international nickel company (INCO). Mechanical milling is a powder processing technique that allows production of homogeneous material starting from blended elemental powder mixtures. This solid state powder processing technique involves repeated welding, fracturing, and rewelding of powder particles in high energy ball mill. Originally developed to produce oxide dispersion strengthened nickel and iron base super alloys for applications in aerospace industry, mechanical milling has been shown to capable of synthesizing a variety of equilibrium and non-equilibrium alloy phases starting from blended elemental or prealloyed powders. The non-equilibrium phases synthesized include supersaturated solid solutions, metastable crystalline and quasicrystalline phases, nanostructures, and amorphous alloys [Suryanarayana 1999, 2001].

The actual process starts with mixing of the powders in right proportion and loading the powder mixture in to the mill along with the grinding medium (Generally steel balls). This mix is then milled for desired period of time until a steady state is reached when the composition of every powder particle is same as the proportion of the elements in the powder mix. Some of the attributes of the process are as follows

- Extension of solid solubility limits
- Development of amorphous phases
- Production of fine dispersion of second phase(usually oxide) particles
- Refinement of grain size down to nanometer range
- Synthesis of novel crystalline and quasicrystalline phases
- Disordering of ordered intermetallics
- Inducement of chemical reactions at low temperatures
- Possibility of alloying of difficult to alloy elements
- Scaleable process

1.2.1. RAW MATERIALS

The raw materials used for milling are widely available commercially pure powders that have particles sizes in the range of 1-200μm. But, the powder particle size is not very critical, except that should be smaller than the grinding ball size. This powder particle size decreases exponentially with time and reaches a small value of a few microns only after a few minutes of milling. The raw powders fall in to the broad categories of pure metals, master alloys, prealloyed powders, and refractory compounds. Ductile-ductile, ductile- brittle, and brittle-brittle powder mixtures are milled to produce navel alloys.

Occasionally, metal powders are milled with a liquid medium and this is referred as wet grinding. If no liquid is involved then it is referred as dry grinding. It has been reported that wet grinding method is more suitable method than dry grinding to obtain fine-ground products because the solvent molecules are adsorbed on the newly formed surfaces of particles and lower their surface energy. The less-agglomerated condition of the powder particles in the wet condition is also a useful factor. It has been reported that the rate of amorphization is faster during wet grinding than during dry grinding. A disadvantage of wet grinding is the increased contamination of powder.

1.2.2 PROCESS VARIABLES

Mechanical milling is a complex process and hence involves optimization of a number of variables to achieve the desired product phase and/ or microstructure. Some of the important parameters, that have an effect on final constitution of the powders, are

- Type of mill
- Milling container
- Milling speed
- Milling time
- Type, size, and size distribution of grinding medium
- Ball to powder weight ratio
- Extent of filling the vial
- Milling atmosphere
- Process control agent, and
- Temperature of milling

All these process are not completely independent. Even then, we will discuss the effect of these variables, assuming mostly that the other variables have no significant effect on the specific variable being discussed, on the final product obtained after milling.

Types of Mills

Different types of high energy milling equipments are used to produce mechanically alloyed powders. They differ in their capacity, efficiency of milling and additional arrangements for cooling, heating, etc. A brief description of different mills is provided below.

A. SPEX Shaker Mills

Shaker mills such as SPEX mills which mill about 10-20 grams of powder at a time, are most commonly used for laboratory investigations and for alloy screening purposes. The common variety of the mill has one vial, containing the sample and grinding balls, secured in the clamp and swung energetically back and forth several thousand times a minute.

The back and forth shaking motion is combined with lateral movements of the ends of the vial. Because of the amplitude (about 5cm) and speed (about 1200 rpm) of the clamp motion, the ball velocities are high (of the order of 5m/s) and consequently the force of ball's impact is great. Therefore these mills are considered as high energy variety.

B. Planetary Ball Mills

Another popular mill is the planetary ball mill (referred to as pulverisette) in which a few hundred grams of powder can be milled at a time. The planetary mill owes its name to the planet-like movement of its vials. These are arranged on a rotating support disk and a special drive mechanism causes them to rotate around their own axes. The centrifugal force produced by vials rotating around their own axes and that produced by the rotating support disk both act on the vial contents, consisting of material to be ground and the grinding balls. Since the vials and the supporting disk rotate in the opposite directions, the centrifugal forces alternatively in like and opposite directions. This causes the grinding balls to run down the inside wall of the vial – the friction effect, followed by material being ground and the grinding balls

lifting off and traveling freely through the inner chamber of the vial and colliding against the opposite inside wall – the impact effect (fig 1.18a & b)

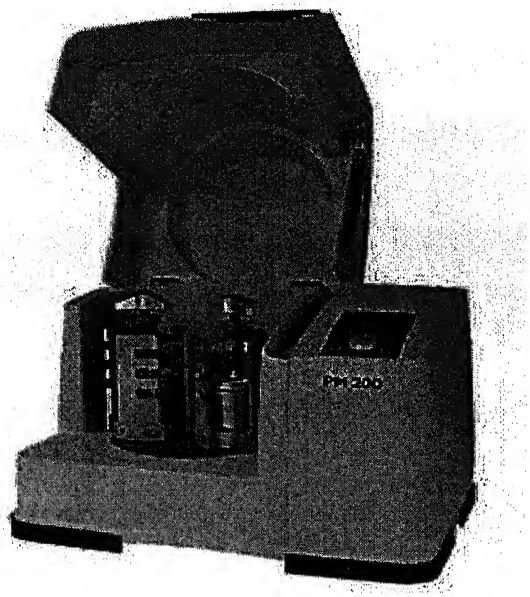

(a)

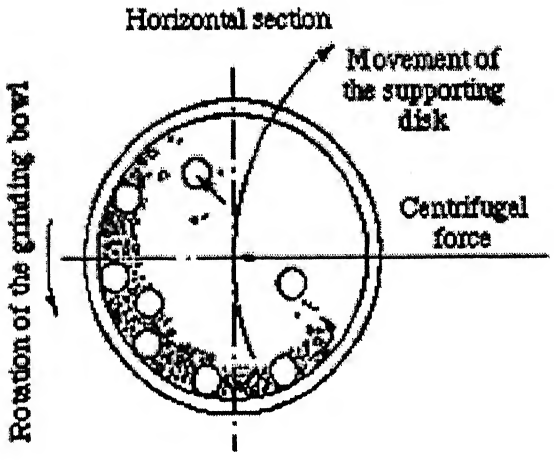

(b)

Figure 1.18 (a) Fritch Pulverisette P-5 four station ball mill. (b) Schematic depicting the ball motion inside the ball mill (Courtesy of Gilson company. Inc.Washington, OH.)

C. Attritor Mills

A conventional ball mill consists of rotating horizontal drum half-filled with small steel balls. As the drum rotates the balls drop on the metal powder that being

ground. The rate of grinding increases with the speed of rotation. Attritors are the mills in which large quantities of powder (from about 0.5 to 40 kgs) can be milled at a time.

New Designs

Several new designs of mills have been developed in the recent years for specialized purposes. These include the rod mills, vibrating frame mills, and the equipment available from Dymatron Cincinnati, OH; Super Misuni NEV – MA – 8 from Nisshin Giken, Tokyo, Japan (with ability to control the temperature of milling from very low temperatures by spraying liquid nitrogen up to a high temperature 300°C by electrical heating); Uni-ball-mill from Australian Scientific Instruments (it is possible to control the nature and magnitude of impact of the balls in this machine by controlling the field strength with the help of adjustable magnets) etc.

Milling Container

The material used for the milling container is important because if the material of the grinding vessel different from that of the powder, then the powder may be contaminated with the grinding vessel material during grinding. The shape of the container also seems to be important, especially in the internal design of the container. Alloying was found to occur at significantly higher rates in the flat ended vial than the round ended container

Milling Speed

It is easy to realize that the faster the mill rotates the higher would be the energy input in to the powder. But, depending on the design of the mill there are certain limitations to the maximum speed that could be employed. In the conventional mill there is an upper speed limit and that could be employed. In the conventional mill there is an upper speed limit and if the speed is increased above this critical speed (upper limit), the balls will be pinned to the inner walls of the vial and do not fall down to exert any impact force on the powder. Therefore, the maximum speed should be well below the critical speed so that balls fall down from the maximum height to produce maximum collision energy.

Another limitation is that at high speeds, the temperature of the vial may reach a value. This may be advantageous in some cases where diffusion is required to

promote homogenization and/ or alloying in the powders. But, in some cases, this increase in temperature may be disadvantage because the increased temperature accelerates the transformation process and results in the decomposition of supersaturated solid solutions or other metastable phases formed during milling. Additionally, the high temperature generated may also contaminate the powders. It has been reported that during nanocrystal formation, the average crystal size increases and the strain decreases at higher milling intensities due to the enhanced dynamical recrystallization [Surayanarayana 1999, 2001].

Milling Time

The milling time is the most important parameter. Normally the time is so chosen as to achieve a steady state between the fracturing and cold welding of the powder particles. The times required vary depending on the type of the mills used, the intensity of the milling, the ball-to-powder ratio, and the temperature of milling. It should be noted that the level of contamination increases as the milling time is increased hence it is desirable that the powder is milled just for the required duration and not any longer.

Grinding Medium

The density of the grinding medium is high enough so that the balls create enough impact force on the powder. It is always desirable to have the grinding vessel and the grinding medium made of the same material as the powder being milled to avoid cross contamination. The size of the grinding medium also has an influence on the milling efficiency. A larger size (and high density) of the grinding medium is useful since the larger weight of the balls will transfer more impact energy to the powder particles. It has been reported that the final constitution of the powder is dependent upon the size of the grinding medium used.

Ball-to-Powder Weight Ratio

The ratio of the weight of the balls to the powder (BPR),some times referred to as charge ratio (CR), is an important variable in the milling process. This has been varied by different investigators from a value as low as 1:1 to as high as 20:1 . The higher the BPR, the shorter is the time required to achieve a particular phase in the powder being milled. At high BPR more energy is transferred to the powder particles

and so alloying takes place faster. It is also possible that due to higher energy, more heat is generated and this could change the constitution of the powder. The amorphous phase may even crystallize if the temperature rise is substantial [Suryanarayana 2001].

Extent of Filling the Vial

Since alloying among powder particles occurs due to impact forces exerted on them, it is necessary that should be enough space for the balls and powder particles to move around freely in the milling container.

Milling Atmosphere

The major effect of the milling atmosphere is on the contamination of the powder. Therefore, the powders are milled in the container that have been either evacuated or filled with an argon gas such as argon or helium.

Process Control Agents

The powder particles get cold welded to each other, especially if they are ductile, due to the heavy plastic deformation experienced by them during milling. But, true alloying among the powder particles can occur only when balance is maintained between cold welding and fracturing of the particles. A process control agent (PCA), also referred to as lubricant or surfactant, is added to the powder mixture during milling to reduce the effect of cold welding.

The PCAs can be solids, liquids or gasses. They are mostly organic compounds, which act as surface active agents. The PCA adsorbs on the surface of the powder particles and minimizes cold welding between powder particles and thereby inhibits agglomeration. The surface-active agents adsorbed on the particle surfaces interfere with cold welding and lower the surface tension of the solid material. Since the energy required for the physical process of size reduction, E is given by

$$E=\gamma\Delta S$$

Where, γ is the specific surface energy and ΔS is the increase of surface area, a reduction in surface energy results in the use of shorter milling times and/or generation of finer powders [Suryanarayana 2001].

A wide range of PCAs has been used in practice at a level of about 1-5 wt% of the total powder charge. The most important of the PCAs include stearic acid, hexane,

methonal, ethanol, and acetone. The choice of a PCA for milling depends on the nature of the powder being milled and the purity of the final product desired.

Temperature of Milling

The temperature of the milling is another important parameter in deciding the constitution of the milled powder. Since diffusion process are involved in the formation of alloy phases irrespective of whether the final product phase is solid solution, intermetallics, nanostructure, or an amorphous phase, it is expected that the temperature of milling will have a significant effect in any alloy system.

During the formation of nanocrystals, it was reported that the root mean square (rms) strain the material was lower and the grain size larger for materials milled at higher temperatures. For example, during planetary ball milling of a Cu-37at% Ag powder mixture, it was noted that the mixture of an amorphous and crystalline (supersaturated solid solution) phases was obtained on milling at room temperature; instead, only a Cu-8at%Ag solid solution was obtained on milling the powder at 200°C. Similar results were also obtained in the Cu-Ag, Zr-Al, and Ni-Ag alloy systems and were explained on the basis of the increased diffusivity and equilibrium effects at higher temperatures of milling.

1.2.3 MECHANISM OF MECHANICAL MILLING

During high-energy ball milling the powder particles are repeatedly flattened, cold-welded, fractured and rewelded. Whenever two balls collide, some amount of powder is trapped in between them. Typically, around 1000 particles with an aggregate weight of about 0.2 mg are trapped during each collision. The force of impact plastically deforms the powder particles leading to work hardening and fracture (Figure 1.19). The new surfaces created enable the particles to weld together and this leads to an increase in particle size. Since in the early stages of milling, the particles are soft (if we are using either ductile to ductile or ductile-brittle material combination), their tendency to weld together and form large particles is high. A broad range of particle sizes develops, with some as large as three times bigger than the starting particles.

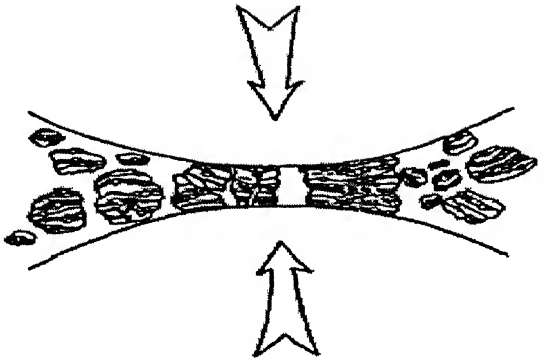

Figure 1.19 Ball powder ball collision of powder mixture during Mechanical milling [Gilman and Benjamin 1983].

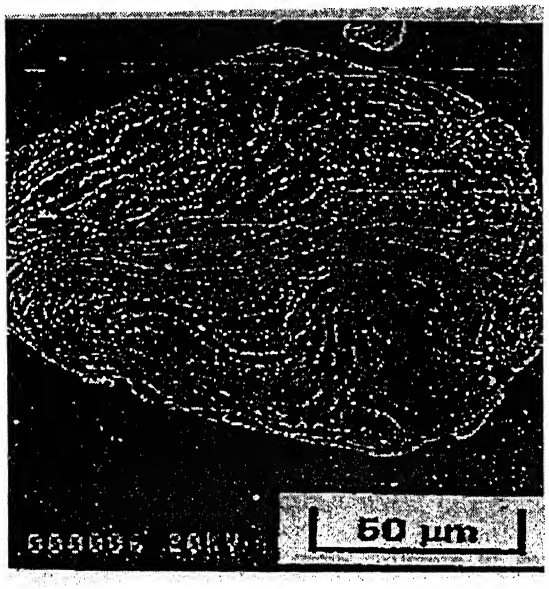

Figure 1.20 Scanning electron micrograph depicting the convoluted lamellar structure obtained during milling of a ductile-ductile component system (Ag-Cu)[Suryanarayana 2001].

This stage has a characteristics layered structure consisting of various combinations of starting constituents (Figure 1.20) [Surayanarayana 1999, 2001]. With continued deformation, the particles get work hardened and fracture by fatigue failure mechanism and/ or by the fragmentation of fragile flakes.

Fragments generated by this mechanism may continue to reduce in size in the absence of strong agglomerating forces. At this stage, the tendency to fracture predominates over the cold welding. Due to the continued impact of the grinding balls, the structure of the particles is steadily refined, but the particle size continues to

be same. Consequently, the interlayer spacing decreases and the number of layers in the particle increases. However, it should be noted that the efficiency of the particle size reduction is very low, about 0.1% in a conventional ball mill. The efficiency may be somewhat higher in high-energy ball milling processes, but is still less than 1%. The remaining energy lost in the form of heat, but a small amount is also utilized in the elastic and plastic deformation of the powder particles.

After milling for a certain period of time, steady state equilibrium is attained when a balance is achieved between the rate of welding, which tends to increase the average particle size, and the rate of fracturing, which tend to decrease the average composite particle size. Similar particles are able to with stand deformation without fracturing and tend to be welded in larger pieces, with an overall tendency to drive both very fine and very large particles towards intermediate size. At this stage each particle contains substantially all of the starting ingredients, in the proportion they were mixed together and the particles reach saturation hardness due to the accumulation of the strain energy. The particle size distribution at this stage is narrow, because particles larger than average size at the same rate that fragments smaller than average grow through agglomeration of smaller particles (Figure 1.21).

From the foregoing it is clear that during MA, heavy deformation is introduced in to the particles. This is manifested by the presence of a variety of crystal defects such as dislocations, vacancies, staking faults, and increased number of grain boundaries. The presence of this defect structure enhances the diffusivity of solute element in to the matrix. Further, the refined micro structural features decrease the diffusion distances. Additionally, the slight rise in temperature during milling further aids the diffusion behavior, and consequently, true alloying takes place amongst the constituent elements. While this alloying generally takes place normally at room temperature, sometimes it may be necessary to anneal the mechanically alloyed powder at elevated temperature for alloying to be achieved. This is particularly true when formation of intermetallics is desired.

The specific times required to develop a grain structure in any system would be a function of the initial particle size and characteristics of ingredients as well as the specific equipment used for conducting the mechanical alloying operation and the operating parameters of the equipment. But, in the most cases, the rate of refinement of the internal structure (particle size, crystallite size, lamellar spacing, etc.) is roughly logarithmic with processing time and therefore the size of the starting particles is

relatively unimportant. In a few minutes to an hour, the lamellar spacing becomes small and the crystallite (or grain) size is refined to nano dimensions (Figure 1.22). The ease with which nanostructured material can be synthesized is one reason why MA has been extensively employed to produce nanocrystalline materials.

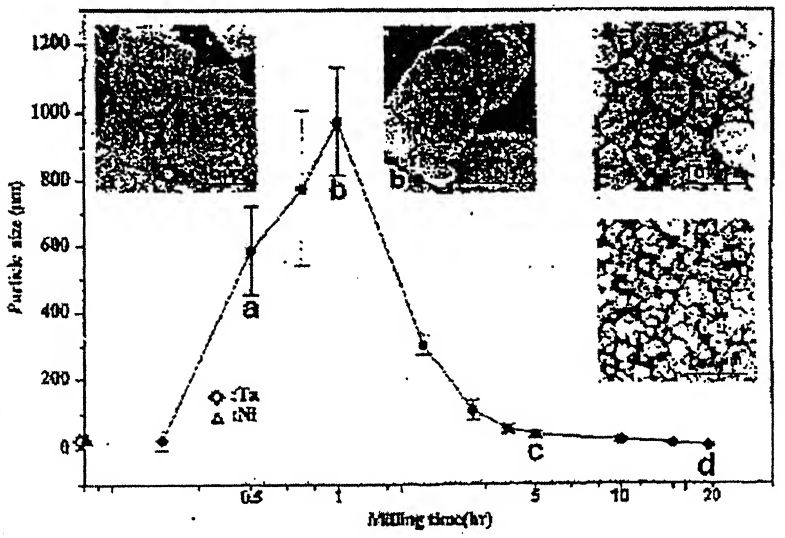

Figure 1.21 Narrow particle size distribution caused by tendency of small particles to weld together and large particles to fracture under steady-state conditions [Suryanarayana 2001].

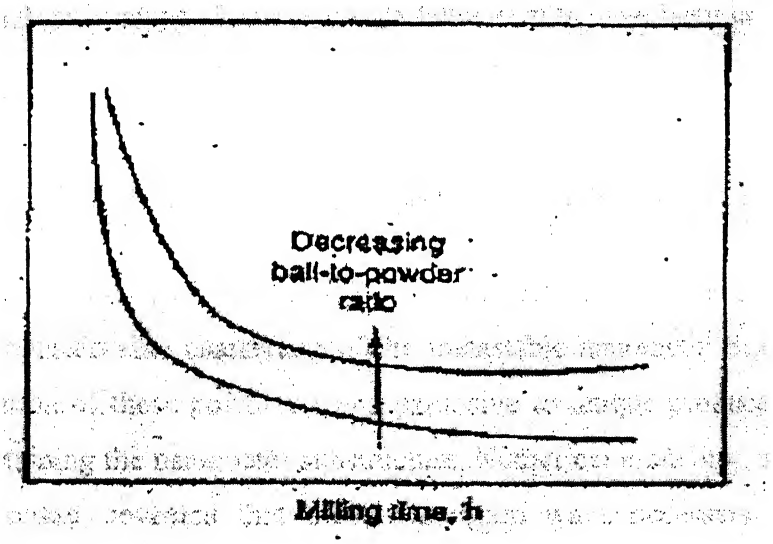

Figure 1.22 Refinement of particle size with milling time

1.2.4 APPLICATIONS OF MECHANICAL MILLING

This technique of have been used to produce a variety of materials. The most important reason for the invention and development of the MA process was the production of oxide dispersion strengthened (ODS) materials in which fine particles of Y_2O_3 or ThO_2 were uniformly dispersed in a nickel or iron based super alloy. Investigations have revealed that MA can synthesize metastable phases such as super saturated solid solutions, nonequilibrium crystalline or quasicrystalline intermediate phases and amorphous alloys. In addition, nanostructures with grain size of a few nanometers, typically <100nm, are produced. These metastable phases have interesting combinations of physical, chemical, mechanical, and magnetic properties and are being widely explored for potential applications.

Mechanically alloyed materials find applications in variety of industries. The applications include synthesis and processing of advanced materials (magnetic materials, superconductors, and functional ceramics), intermetallics, nanocomposites, catalysts, hydrogen storage materials, food heaters, gas absorbers, and also in the modification of organic compounds, waste management, and production of fertilizers. But, the major applications of mechanically alloyed materials have been in the areas of thermal processing, glass processing, energy production, aerospace, and other industries

1.3 NANO STRUCTURED MATERIALS

1.3.1 INTRODUCTION

In the recent years, the nano-technology has been identified as a new wave towards millennium innovations in the materials science and engineering. With the reduction of a characteristic length such as the grain size or the cluster or molecular size, the normal properties of materials were reported to be drastically changed.Nano-stuctured materials can be represented as "a broad class of materials, with microstructures modulated in zero to three dimensions on length scales less than 100nm" or in other words "materials with atoms arranged in nano sized clusters, which become the constituent grain or building blocks of materials". The emerging fields of nanoscale science, engineering and technology – the ability to work at the molecular level, atom by atom, to create large structures with fundamentally new

properties and functions- are leading to unprecedented understanding and control over the basic building blocks and properties of natural man made things.

Scientists have opened a broad net of discoveries that does not leave any major research area untouched in physical, biological, and engineering and sciences. The importance and potential of nanotechnology is quite visible in the words of "Roco" as he predicts "As the 21st century unfolds, nano technology's impact on health, wealth and security of the world's of people is expected to be at least as significant as the combined influences in this century of antibiotics, integrated circuits, and other advanced materials"(Roco 2002). In 2001, virtually all the countries have initiated programs in this area or had national programs in advanced planning (Roco 2001). As shown in table „ the world wide nanotechnology R&D investment reported by the government organizations including Japan , western Europe, and the USA has increased approximately five times in the last 5 years, between 1997 & 2002(Roco 2003).

In the coming years, it can be predicted that the convergence of nano-technology with information technology, modern biology, and social sciences will reinvigorate discoveries and innovations in almost all the areas of economy.

1.3.2 DEFINITIONS AND CLASSIFICATION OF NANOSTRUCTURED MATERIALS

The basic question, which arises during the discussion, is what nano structured materials are at all. In what way these materials should be defined? A number of researchers and Scientists have defined them in different ways. In this section, we will have an overview of these materials including various definitions and their classification

Definitions

About nanocrystalline materials, the pioneering Gleiter says,

Nanocrystalline solids are polycrystals, the crystal size of which is a few (typically 1 to 10) nanometers[Gleiter 1991].

According to R.W.Siegal,

"Nano phase materials are three dimensionally modulated, synthetic materials with average grain size, phase or other structural domain sizes below 100nm"[Siegel 1993].

At another place Gleiter defined NsM as,
"NsM are solids composed of structural element – mostly crystallites – with a characteristic size (in at least one direction) of a few nanometers"[Gleiter 1995].

The designation "nano powder" is usually used to describe powders with a particle diameter less than 1 micrometer (1000nm) [Eifert et al 2000].Some more definitions of NsM are as follows:

(i) According to Lu et al: "Nanostructured materials have characteristic length scale of a few (typically 1-10) nanometers" [Yulin and Liaw2001].

(ii) According to McHenry and Laughin: "the term nanocrystalline alloy is used to describe those alloys that have majority of grain diameters in the typical range from 1 to 50 nanometers"[Mc Henry et al 2000].

(iii) According to R.Birringer: "nanocrystalline materials are single-phase or multiphase polycrystals, the crystal size of which is of the order of a few (typically 1-10) nanometers, so that about 50 volumes % of the material consists of grain or interphase boundaries"[Birringer 1989].

(iv) Gleiter again summarized NsM as,
NsM are materials with microstucture, the characteristic length scale of which is on the order of a few (typically 1-10) nanometers" [Gleiter 2000].

On the basis of above information NsM can be defined as follows:
"NsM are single phase or multiphase polycryastals having the crystal size of the order of a few (typically 1-100) nanometers in at least one dimension".

Classification on the basis of Dimensionality

Nano-structured materials can be classified on the basis of dimensionality (in which length scale is in nanometers) as follows:
(a) nano particles
(b) Layered or lamellar structure
(c) Filamentary structure
(d) Bulk nano-structured materials

Nano particles are atom clusters and can be considered zero dimensional (0-D) in nature [Seigel 1994]. A layered or lamellar structure is a one dimensional (1-D) nano structure in which the magnitudes of length and width are much greater than thickness that is only a few nanometers in size. A two dimensional (2-D) nano-structure can be termed as filamentary and in this the length is substantially larger than width or diameters, which are of the nano dimensions [Suryanarayana 1995]. The

most common nano structure is basically equiaxed (all the 3-dimensions are in nm size) and are termed nano structured crystallites or 3-D nano structures [Suryanarayana and Koch 1999].

The Nano Structured Materials may contain crystalline, quasicrystalline, or amorphous phases and can be metals, ceramics, polymers or composites. If grains are made up of crystals, the material is called nanocrystalline. On the other hand if they are made up of quasicrystalline or amorphous (glassy) phases, they are termed nano-quasi-crystals or nano-glasses [Suryanarayana 1995]. A detailed classification of NsM is shown in Figure 1.23a & b and Table 1.2

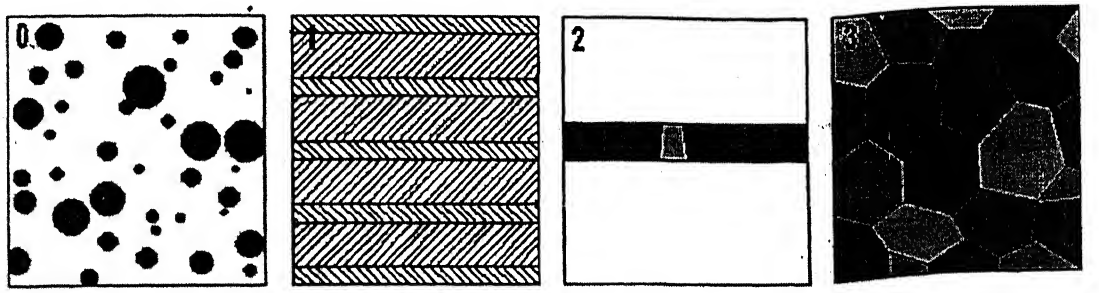

Figure 1.23a Schematic representation of four types of nano crystalline materials [Siegel 1994].

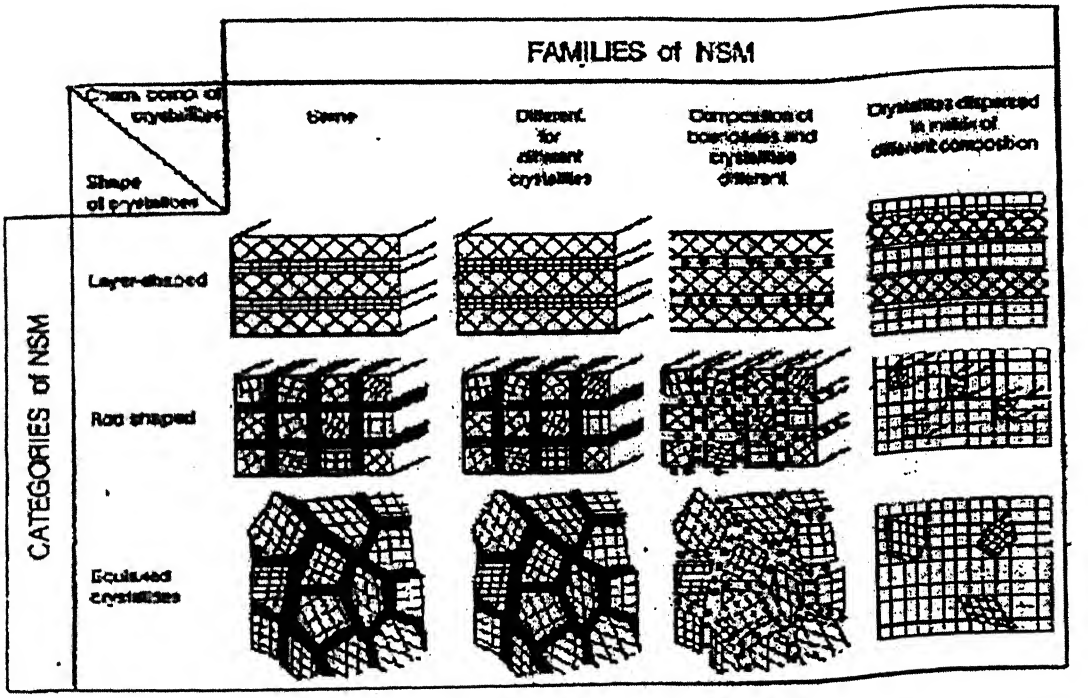

Figure 1.23b Classification Scheme for NsM according to their chemical composition and the dimensionality (shape) of the crystallites (structural elements) forming the NsM[Gleiter2000].

1.3.3 STRUCTURE OF NANOCRYSTALLINE MATERIALS

The microstrustural features of importance include (a) Grain size, grain size distribution and morphology, (b) the nature and morphology of grain boundaries and interphase and morphology, (c) the perfection and nature of intra-grain defects, (d) composition profile across grains and interfaces, and (e) identification of residual trapped species from processing.

There is a gamut of experimental techniques that can yield structural information on nanocrystalline materials. These include 'direct; microscopic techniques such as transmission electron microscopy (TEM), scanning tunneling microscopy (STM), atomic force microscopy (AFM), field ion microscopy (FIM), and less direct electron, X-ray and neutron diffraction techniques. Indirect spectroscopic tools, such as EXAFS, nuclear magnetic resonance, Raman and Mossbauer spectroscopies, and positron annihilation spectroscopy, have also been used. Owing to the ultrafine scale of nanocrystalline materials, traditional characterization tools such as TEM and X-Ray diffraction technique are both necessary and useful to understand the structure of nanocrystalline materials.

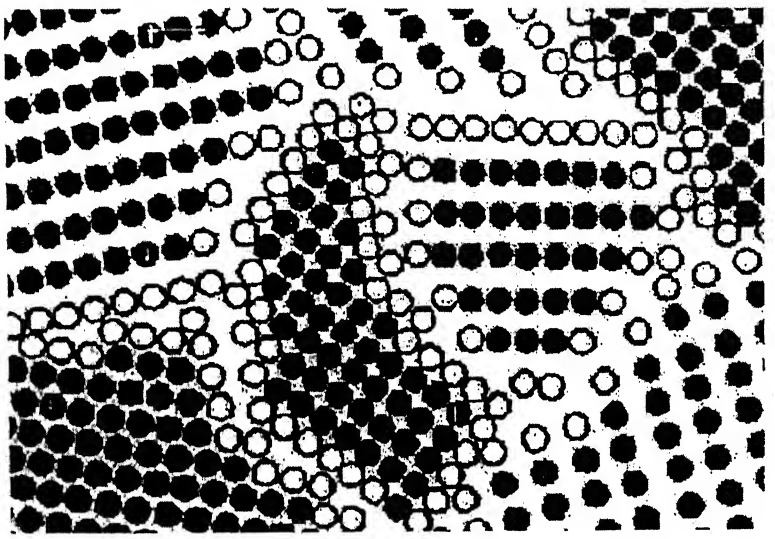

Figure 1.24 Schematic arrangements of atoms in equiaxed nano crystalline metal

A nanocrystalline metal contains typically a large number of interfaces with random orientation relationship, and consequently a substantial fraction of the atoms lies in the interfaces (Figure 1.24). Assuming that grains have the shape of the spheres or cubes, the volume fraction of atoms associated with the boundaries can be calculated as follows [Andrievski 2002]:

$$V_f=3S/D$$

Where,

S= average grain boundary thickness

D= average grain diameter

It has been observed that volume fraction of atoms in the grain boundaries can be about 50% for 5 nm grains, decrease upto30% for 10 nm grains and 3% for 100 nm grains. Nanocrystalline metals can be considered to consist of two structural components – the numerous small crystallites with long range order and different crystallographic orientations constituting the "crystalline" component and a network of intercrystalline regions, the structure of which differs from region to region: which is referred as the "interfacial" component [Koch 1999].

Atomic Structure of Crystal Lattice and the Grain Boundary

The structure of the grains (crystallites) in nanocrystalline materials has been accepted to be the same as in a coarse-grained materials i.e long range order atomic structure [Gleiter2000]. Initially it was suggested that nanocrystalline grain boundary atomic structure has "gas like disorder". But after exhaustive studies on the nature of grain boundary structure, it has been established in most of the cases that interface structures are remarkably close, structure wise, to those in conventional crystalline materials with micron sized grains [Ranganathan etal 2001].

Triple Junction and Higher Order Grain Junction

In the ultra fine grained (nanocrystalline) materials, triple junctions and higher order junctions become an important component of the microstructure. The total intercrystalline region consisting of grain boundaries, triple junctions and four grained points is more important than just the grain boundary. The grain boundary area is inversely proportional to the grain size while triple line length is proportional to Inverse Square of the grain size. Thus the contribution of triple junction and higher order grain junction becomes important at very small grain size [Koch 1997].

1.3.4 CONSOLIDATION STRATEGY FOR NANO STRUCTURED MATERIALS

The potential application of nanoscale materials as novel structural or functional engineering materials largely depends on the consolidation of powders into bulk nanoscale solids. The retention of metastable microstructure in the course of this

consolidation process is essential for preserving the often superior mechanical, magnetic, or catalytic properties of the material [Gleiter 2000]. Consolidation of the nanocryatlline powders has been achieved by **electro-discharge compaction; plasma activated sintering , explosive consolidation, hot isostatic processing, hydrostatic extrusion, strained powder rolling and sinter forging** [Suryanarayana 1999, Siegel 1994].

Optimization of consolidation parameters is important because retention of nanostructures requires use of low consolidation temperatures while achieving full (theoretical) density requires use of high temperatures [Ma and He 2000]. However, it should be noted that because of the increased diffusivities in nanocrystlline materials, sintering takes place at a temperature much lower than in coarse-grained materials. This is likely to reduce the grain growth. It is typically difficult to obtain full density while retaining the nanoscale microstructure. The high driving force and enhanced kinetics due to large curvature facilities may cause full densification of nanocrystalline materials at temperatures below those of coarse grained materials of the same composition by few hundred degrees [Ma 2000, Ma and He 1996]. Retention of fine grain sizes and elimination of sintering aids are specific advantages of the lower processing temperatures [Liu 1998, Suraynarayana and Hofler et al 1993].

Effect of Temperature on Consolidation

For conventional materials, pores are removed through sintering at high temperatures for long times, driven by the reduction in surface energy where as for nanophase materials, consolidation temperature needs to be kept low to maintain nanoscale grain sizes. Full densification is possible at some intermediate elevated temperatures because nanophase powders are expected to show increased sinterability compared with their conventional coarse-grained counterparts. A reduction in sintering temperature can reduce contamination and compositional changes, and stresses and cracking during cooling. A number of factors contribute to this possible processing advantage. For mechanically milled powders, particles with varying sizes may lead to easier filling of pores of different sizes. Fine grain sizes provide shorter diffusion paths and much increased densification rate during sintering [Ma 2000].

It is obvious that the diffusional processes that mediate sintering also lead to undesired grain growth. The driving force for grain growth also increases, as grain

size decreases such that the advantage nanophase materials have in sinterability can be partly lost due to concomitant grain growth that destroys the desirable nanoscale grain size. Therefore, consolidation temperature needs to be maintained sufficiently low, and other mechanisms (such as stress assisted densification) must be invoked to allow full consolidation and retention of nanostructure.

Effect of Pressure on Consolidation

To compensate for the low consolidation temperature the strategy usually adopted is to use hot pressing and forging employing high pressure (of the order of 0.5-1.0 GPa) to enhance the contribution of plastic deformation and bonding. The high stress enhances the plastic strain controlled pore closure. Also, the stress plays a significant role in stress assisted densification (diffusion) mechanisms. Possible stress effect on deformation and densification can be seen from the established formula for creep, in general.

$$\partial\varepsilon/\partial t = A\sigma^n/RTd^{q^*}\exp(-Q/RT)\, f(\rho)$$

Where, σ is the applied stress, d the grain size, $\partial\varepsilon/\partial t$ the strain rate, n= the stress exponent, q the grain size dependent exponent, A, a coefficient involving diffusivity prefactor, Burger vector, shear modulus etc., Q the activation energy for the accommodation process, ρ the density, R the gas constant, and T the temperature. In this expression, A,n,q, and Q can have different values for different creep mechanisms (Nabarro-Herring creep, Coble creep, Dislocation climb power law creep etc.) and $f(\rho)$ accounts for density effects.

The equation indicates that the high pressure applied and the strong grain size dependence of creep deformation can contribute significantly to densification by plastic deformation at relatively low temperatures. In addition, the extensive plastic deformation under high stress results in disruption of any continues surface oxides on powder particles, which may degrade bonding and properties. The high pressure applied may also have the beneficial effects of slowing down grain growth because of the reduction of free volumes in grain boundaries, which facilitate atomic jump across the boundary.

\

Effect of Contamination

Surface contamination is inevitable for any powder material and may become significant in nanopowders due to their large surface area. Metastable powders

obtained by mechanical alloying or milling are special case. Their structure is either amorphous or nanocrystalline but the powder particle size is in the micron range. In this case, the surface area is less than for nanometer powder particles but contamination is due to large impurity intake during the milling process. Oxides, nitrides and other compounds are often found in consolidated parts made of attrition-milled nanopowders.

Studies show that ultra clean nanoparticles sinter very rapidly even at room temperature. The oxygen contamination decreases the surface energy and slows down the sintering kinetics. To reduce contamination, all mechanical alloying and consolidation should be performed under inert atmosphere. To reduce metallic impurities acquired during milling, milling media and materials being milled should match in composition.

Suppression of Grain Growth

Compared with the grain sizes in as milled powder, grain growth is observed in all consolidation techniques. Grain growth occurs in polycrystalline materials to decrease the system energy by decreasing the total grain boundary energy. Grain growth can be measured by following expression [Gleiter2000]:

$$D^{1/n} - D_0^{1/n} = kt$$

Where,

D = length scale or mean grain diameter

n = empirical constant =<0.5

D_0 = length scale or mean grain diameter at t =0

K = temperature dependent rate parameter, t = annealing time

By applying, $k = k_0 \exp(-Q/RT)$, activation energy Q can be calculated and which in turn can be used to deduce the grain growth mechanism.

Nanocrystalline metals exhibit crystal growth at elevated temperatures. In metals with a crystal size of about 10nm, significant crystal growth (doubling the crystal size in about 24 hours) was noticed at ambient temperature or below equilibrium melting temperature, T was lower than about 600°C.However, if T was higher, the stability against grain growth seems to be enhanced [Gleter 1989]. The grain growth in mechanically alloyed solid solution has been found to decrease with increasing solute concentration, and heat release upon annealing indicates that solute

segregates to the grain boundaries, thereby reducing the specific grain boundary energy and impeding the grain growth [Krill et al 1995].

. There could be several possible ways for suppression of runaway grain growth during consolidation. First of all, sinter forging scheme allows full density processing at relatively low temperatures, significantly below 0.5Tm, resulting in less grain growth than other consolidation methods, second, a minute amount of impurities picked up during milling, although often below the detection limit, may have also contributed to the success in suppressing grain growth through solute drag or Zener drag mechanism. These trace impurities are uniformly distributed by the milling action, reducing the possibility of abnormal grain growth.

Grain size stability is especially high when a second element is added.The solute drag effect, due to the solute atoms segregating to grain boundaries, retards grain growth. iron occurs inside the nanograins or along the abundant grain boundaries. The new grains thus start out with sizes smaller or atleast similar to those in the nanocrystalline precursor phase. Rresultant two phase mixture configuration also helps to isolate grains and/or domains of the same structure and there by reduce grain growth boundary migration. In other words, incorporating a second phase or elements helps to retain nano phase grain size when reaching full density.

Diffusion and Sinterability

Since nanocrystalline materials contain a very large fraction of atoms at the grain boundaries, the numerous interfaces provide a high density of short circuit paths for diffusion. As a consequence, they exhibit an enhanced diffusivity in comparison to with single crystal or conventional coarse-grained polycrystalline materials with the same chemical composition [Schumacher et al.1989, Holfer 1993].

This enhanced diffusivity can have a significant effect on mechanical properties such as creep and superplasticity, ability to dope efficiently nanocrystalline materials with impurities at relatively low temperatures, and synthesis of alloy phases in immiscible metals and the at much lower than those usually required in other systems. The enhanced

Self and impurity diffusivities in nanocrystalline materials appear to be strongly linked to the porosity present in the samples. However, in the light of recent results, the difference in diffusion coefficients seems to be caused by differences in relaxation states rather than by porosity [Holfer 1993].

Solid solubility limits are usually enhanced when the material is in the nanocrystalline state and this has been explained on the basis of elastic strains at the interfaces. The high diffusivity results in alloying, by diffusion along grain boundaries resulting in the formation of stable and metastable phases at relatively low temperatures. Another important consequence of the increased diffusivity is that sintering of nanocrystalline powders can occur at temperatures lower than those required for coarse-grained polycrystalline powders.

1.3.5 PROPERTIES OF NANO STRUCTURED MATERIALS

Due to the fine grained structure, nanocrystalline materials have unique properties that are different and considerably improved in comparison with those of conventional coarse grained polycrystalline materials. These include increased strength and hardness, enhanced diffusivity, improved ductility and toughness, reduced density, reduced elastic modulus, higher electrical resistivity, increased specific heat, higher thermal expansion coefficient, lower thermal conductivity, and better soft magnetic properties in comparison with conventional coarse-grained materials. A brief review of the mechanical properties of nanostructured materials is given in the following section

Mechanical Properties

The elastic constants of nanocrystalline materials have been found to be reduced by 30% or less. The presence of extrinsic defects e.g. pores and cracks, was suggested as the possible reason for low values of Young's modulus in nanocrystalline materials compacted from powders [Krstic 1993].

The Hall-Petch relation for conventional coarse-grained polycrystalline materials suggests that the yield strength (or hardness) of a material increases with a decreasing grain size according to the relationship,

$$\sigma = \sigma_0 + k_H d^n$$

where, d=grain size, σ = 0.2% yield strength (or hardness),

σo = lattice friction stress to move individual dislocations (or the hardness of a single crystal specimen, d$\rightarrow$ infinity)

n = the grain size exponent (generally -1/2), k_H = Hall-Petch intensity parameter

At extremely fine grain sizes, e.g. in the nanometer regime, the individual grains cannot support more than one dislocation; and thus, the Hall-Petch relation may not

be valid. The deviation from the Hall-Petch relationship in nanocrystalline materials may be due to the following reasons:

a) Since in nanocrystalline materials, pile-ups can not form when the grain size is less than a critical value d_c, weaking mechanisms (e.g. viscous type flow) operate and leads to a decrease in hardness with decreasing grain size, i.e. a negative value for the slope k_H.

b) A large number of triple junctions may be a reason for negative slope in nanocrystalline materials as an increased triple junction volume fraction leads to softening and enhanced bulk ductility in polycryastlline materials [Palumbo et al. 1990 Nieh et al. 1991].

Summery of the mechanical properties of nanocrystalline materials can be given as follows [Suryanarayana and Koch 1999].

(1) Except for very small grain nanocrystalline samples (<5 nm) the elastic properties are essentially identical to those of coarse-grained materials.

(2) High hardness and yield strength values are observed for nanocrystalline materials.

(3) Ductile coarse-grained materials are less ductile, perhaps brittle as nanocrystalline materials.

(4) Brittle coarse-grained materials may exhibit slight ductility when nanocrystalline.

(5) Superplasticity has not been observed at low temperatures (<0.4 to 0.5 Tm) for nanocrystalline materials, although it has been observed at somewhat lower temperatures and higher strain rates as grain size is decreases.

(6) Shear bending and perfectly plastic behavior have been seen in some nanocrystalline materials analogous to plastic deformation in amorphous materials

EXPERIMENTAL PROCEDURE

2.1 STARTING POWDER CHARACTERISTICS

2.1.1 Powder morphology

Fig 2.1 & 2.2 show the SEM image of starting W and Ni powders respectively. It is seen that initial W powder particles have spheroidal morphology and the particles are agglomerated whereas initial Ni powder have irregular morphology and are not agglomerated.

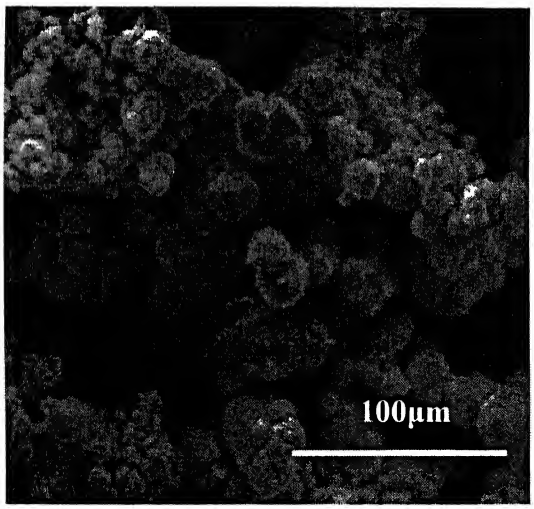

Fig 2.1

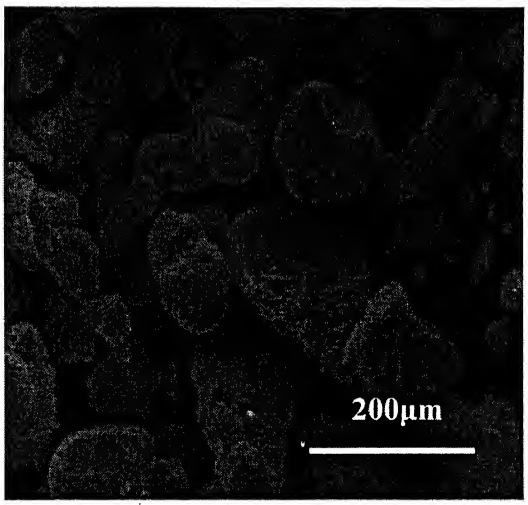

Fig 2.2

2.1.2 Particle size

From the particle size measurement of starting powder it is seen that the mean particle size of Ni is 152.2 µm and that of W is 16.8 µm which is fairly small compared to Ni.It is seen from the histograms showing the particle size, fig 2.3 (a) & (b) that both the powder particles show a wide range of size distribution.

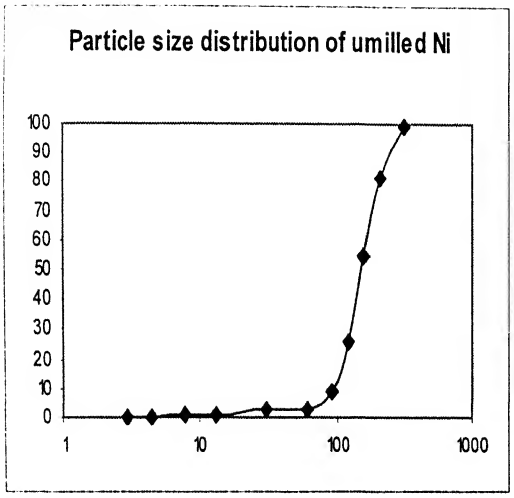

Fig 2.3 (a) Unmilled Nickel powder

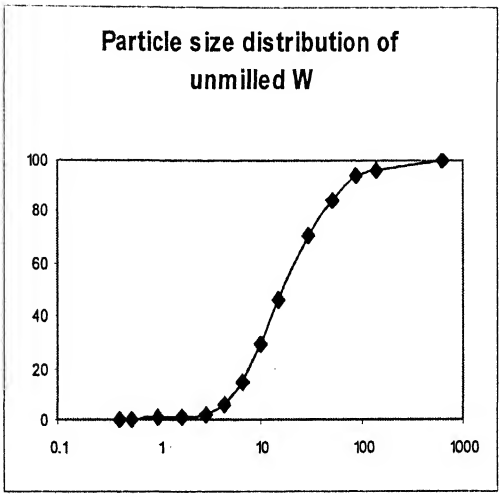

Fig 2.3 (b) Unmilled Tungsten powder

2.2 POWDER MILLING

Ni and W powders, greater than 99.9% purity, weighed separately corresponding to Ni-10wt%W and Ni-30wt%W, were milled in Retsch Planetary Ball Mill (fig 2.2). W-carbide jars and balls were used for this purpose. Each milling batch of above compositions comprised of 24gms of powder. Charge to ball ratio was kept fixed at 1:8 each time. Milling speed was kept at 200 rpm. Acetone was used as the milling media.

For the purpose of monitoring the progress of milling and/or alloying in the powder the milling operation was intermittently stopped after milling time of 5, 15, 25,40,60,80,100,120 and 160 hrs, and very small amount of powder sample was taken out for characterization. Milling time for Ni-30wt%W and Ni-10wt%W powders were 160 and 60 hrs respectively.

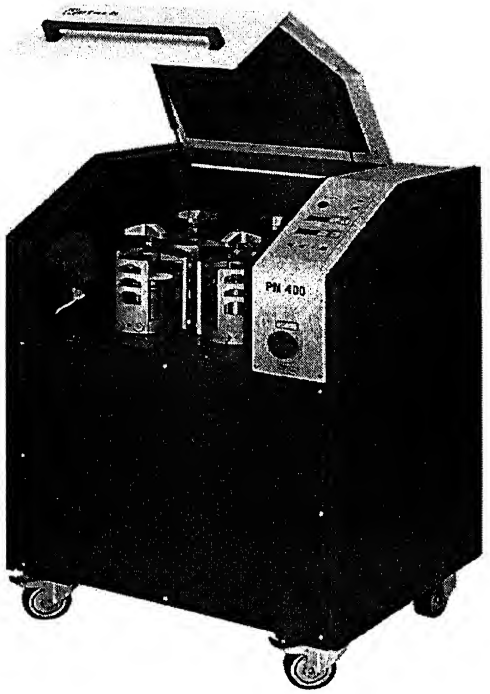

Fig 2.4 RETSCH PLANETARY BALL MILL

2.3 X-RAY DIFFRACTION

Powder samples taken out of the planetary ball mill after different time intervals, and were characterized using X-ray diffraction technique. XED patterns were also taken for sintered single layered and bilayered strips. The instrument used for this purpose was Seifert ISO-DEBYFLEX 2002 diffractometer with copper target. The tube was operated at 30kV and 10mA. The radiation used was Cu Kα having wavelength of 1.540598 A°. The scanning rate in the X-ray powder diffraction was kept at 3°/min and 0.3°/min.

Crystallite Size Determination of Milled Powders

From the XRD pattern 2θ and FWHM (full width at half maximum) values corresponding to the maximum peak is obtained. Since broadening of peak occurs due to grain size reduction and instrumental effect, in order to remove the instrumental broadening effects from the FWHM, the following procedure was adopted. The FWHM value (of the peak at same position as in our sample under investigation) of standard Si sample is eliminated from the FWHM value of sample under investigation by following approximation:

$$B = (W^2 - W_s^2)^{1/2}$$

Where, B is full width at half maximum after suitable correction, W is the FWHM of the sample under consideration and W_s is the FWHM of standard, Silicon in the present case.

The value of B thus obtained is put in the Scherrer's formula to calculate the value of crystallite size which states that,

$$D = K\lambda / (B^*\text{Cos}\theta)$$

Where K is Scherrer's constant, λ is wavelength of copper Kα radiation; θ is half of the value of 2θ in radians.

2.4 SCANNING ELECTRON MICROSCOPY

Powder morphology of mechanical milled powders was analyzed using FEI Quanta 200 Scanning Electron Microscopy (SEM). The milled powder morphologies were observed by sprinkling very small quantity of powder over double adhesive carbon tapes sticked on metallic stubs.

2.5 PARTCLE SIZE ANALYSIS

Particle sizes of powder milled for different lengths of time are measured using the particle size analyser- MARTERIZER 2000. Analysis was done in wet method using water as the dispersant.

2.6 POWDER COMPACTION

The production of compacts from milled powders includes the following procedure: Milled powders were filled in a 1″ * 1″ die which was pressed in the APEX Hydraulic Press under a pressure of 250 Kg/cm^2. The height of the compacted strips was 4-6 mm on an average. Both single and bilayered strips were produced by this method. The single layered strips were produced from powders having composition as Ni-10wt%W & Ni-30wt%W milled for different lengths of time ; while the bilayered strips have one layer of unmilled pure Ni and other layer of milled Ni-10wt%W or Ni-30wt%W powders.

2.7 SINTERING OF COMPACTED STRIPS

Compacted strips were sintered in controlled atmosphere tubular furnace at a temperature of 900°C for 90mins (soaking time) followed by furnace cooling. . The furnace was flushed with argon gas before inserting the samples.Entire sintering operation was carried under hydrogen atmosphere.

2.8 COLD ROLLING OF SINTERED STRIPS

The single and bilayered sintered strips were cold rolling followed by sintering/annealing cycles. The total percent reduction during rolling in each cycle was varied, keeping percent reduction per pass not greater than 5%. Sintering of rolled strips was done in at 900°C for 30 mins in tubular furnace under hydrogen atmosphere.

Single Layered Strips:

The total percent reduction given during rolling in each cycle to strip made from Ni-10wt%W powder milled 60 hrs are 49%, 37%, 50% and 38%.

Strip made from Ni-30wt%W milled 60 hrs could be given a percent reduction of 10% before fracture.

Bilayered Strips:

The total percent reduction given during rolling, in each cycle, to strip having:

a) Ni-10wt%W powder milled 25 hrs as one layer & pure unmilled Ni as the other are 38%, 51% and 42%

b) Ni-10wt%W powder milled 40 hrs as one layer & pure unmilled Ni as the other are 35%, 42% and 40%

c) Ni-10wt%W powder milled 60 hrs as one layer & pure unmilled Ni as the other are 30%, 34% and 32%

The total percent reduction that could be given before fracture to strips having Ni-30wt%W milled for 60hrs (and above) as one layer and pure unmilled Ni as other layer was only about 8-10% out of which reduction of Ni layer was about 20-25% Ni-30wt%W layer was only 2-3%

2.9 DENSITY MEASUREMENT

Density is obtained from mass and volume measurements of the material under study applying the formula, $\rho=M/V$; where ρ= density, M=mass & V=volume. . The materials in this case are the sintered samples and the samples obtained after final rolling. Mass is directly measured using digital Denver Weighing Instrument. Volume is measured by weight loss method applying Archimedes Principle.

2.10 OPTICAL MICROSCOPY

Small pieces were cut from sintered strips for microstructural studies. Sample preparation involved hot mounting of the sintered pieces followed by polishing in emery paper from course to fine and finally in fine cloth with 0.3 μm alumina abrasive in suspension with water. Samples were cleaned and dried, followed by imaging in the Axioskop 2 MAT optical microscope equipped with image grabbing and analysis facility. Similar procedure was used for microstructural studies of rolled strips.

2.11 HARDNESS TESTING

Hardness values of the single and bilayered strips after rolling were determined using CARL ZEISS JANA GERMANY 160 Microhardness Tester. The hardness values of the powders were determined under 20gm of load. Microhardness, μH, was calculated using the formula:

$$H = 1854\ P/\ D^2 \text{ in } Kg/mm^2$$

Where, P is the load in gms and D is the average length (in μm) of the two diagonals of the indentation

2.12 TENSILE TESTING

Tensile tests were performed on dog bone samples obtained from final rolled single and bilayered strips.The instrument used for tensile testing was INSTRON 1195.

Tests were performed at a strain rate of 0.025 mm\min; uniaxial load applied was 2 KN.

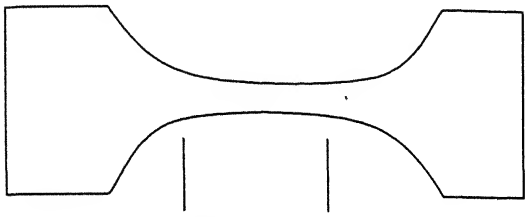

Sample Dimensions

Sample I: gauge length=20.00mm, c/s area=1.08mm^2

Sample II: gauge length 19.86, c/s area=1.14 mm^2

Sample III: gauge length 19.14, c/s area=1.27 mm^2

Sample I: Single layer strip; Ni- 10 wt% W- milled 60 hrs Sample II: Bilayered strip; Ni- 10 wt% W- milled 25 hrs + unmilled Ni Sample III: Bilayered strip; Ni- 10 wt% W- milled 40 hrs + unmilled Ni

2.13 FRACTOGRAPHY

Fracture surface of samples after tensile test were examined using FEI Quanta 200 Scanning Electron Microscopy (SEM).

RESULTS AND DISCUSSIONS

3.0 INTRODUCTION

While nickel crystallizes in the face centered cubic (fcc) crystal structure tungsten crystallizes in the body centered cubic (bcc) structure. However, as shown in Figure1.9, nickel can form a solid solution containing about 20 wt% tungsten. Single phase nickel based alloys having solid solutions of Ni-W have been prepared by the conventional processing route involving melting and solidification. In contrast, till today not much research has been reported related to the study of powder behavior and characteristics during mechanical milling of Ni - W powders. In order to see (i) the milling behavior in the Ni-W system and (ii) whether any mechanical alloying takes place in the Ni-W system or not, the present work was undertaken as part of the present study. As mentioned in Chapter 3, powders of compositions of Ni-10 wt% W and Ni- 30 wt% W were studied by high energy milling in a planetary ball mill.

Even if no mechanical alloying is achieved, tungsten can be used to achieve dispersion strengthening in the Ni-W system. The P/M approach can thus be used for preparing Ni substrates of higher tensile and yield strength. From this perspective again mechanical milling for obtaining a very fine dispersion of tungsten particles in a nickel matrix can be considered as a far superior technique compared to manual mixing of powders of Ni and W as it is likely to produce a much finer homogenous powder mixture.

As mentioned earlier, the present study was primarily aimed at making single layered Ni-W or bi-layered Ni - Ni-W strips. Unmilled nickel powder and mechanically milled Ni-10 wt% W and Ni-30 wt% W powders were used for this purpose. The results described in this chapter elaborate (a) powder characteristics of milled Ni-10 et% W powder for the milling time up to 60 hours and Ni-30 wt% W powder up to the milling time of 160 hours, (b) consolidation behavior of milled Ni-W powders for producing single layered Ni-W strips and bi-layered Ni - Ni-W strips and (c) mechanical properties of the consolidated strips in a few cases.

3.1 CHARACTERISATION OF MECHANICALLY MILLED POWDERS

3.1.1 Nickel-Tungsten Dispersion or Mechanical Alloying

X-ray diffraction (XRD) pattern is a useful tool to determine the progress of alloying in a given elemental powder system during its milling. For this purpose, high intensity peaks corresponding to diffraction from the constituent elements (in the present case Ni and W) were monitored with respect to milling time. The standard 2θ values and the corresponding peak intensities for pure Ni and W, as obtained from the standard JCPDS files, are shown in Tables 3.1 and 3.2 respectively. Identification of phases formed during the course of milling was done using these values as the standard values.

The XRD patterns of Ni-30 wt% W powder milled for 5, 15, 25, 40, 60, 80, 100, 120 & 160 hrs are shown in Figures 3.1(a) and (b). The 2θ values corresponding to peak intensities were obtained from each pattern and compared with the standard 2θ values at which peak intensities are obtained for Ni and W. As an example the 2θ values and corresponding peak intensities of 160 hrs milled powder is shown in Table 3.3. A comparison with standard 2 θ values shows that both Ni as well as W exist in the milled powder more or less in their elemental form and no new phase forms in the system due to mechanical alloying. The absence of any peak corresponding to oxides of Ni and/or W also shows that the milling could be done essentially without any oxidation or contamination of constituent powders.

The XRD patterns obtained from Ni-10 wt% W powder mixture milled for 25, 40 and 60 hrs respectively are shown in Figure 3.2. A similar procedure of analysis of the XRD patterns, as for the patterns of Ni-30 wt% W milled powders, was adapted for Ni-10 wt% W powder. It is seen that in this case also Ni and W powders essentially remained as elemental constituents, no new phase was formed due to mechanical alloying and both Ni and W powders suffered from their oxidation or contamination in any significant manner. A comparison of the pattern of 160 hrs milled sample with that of pure Ni and W is also shown in Figure 3.3.

The above results clearly show that the mechanical alloying during high energy milling of Ni and W powders corresponding to 10 wt% W and 30 wt% W does not occur up to the milling time of 160 hours in Ni-30 wt% W system and up to the milling time of 60 hours in the Ni-10 wt% W system. Both Ni as well as W are

retained in the powder as elemental constituents and are expected to form as a fine dispersion.

Table 3.1 Intensities, 2θ values and corresponding planes of tungsten collected from 2001 JCPDS

2θ	INTENSITY	h k l
40.23	100	1 1 0
58.33	15	2 0 0
73.27	23	2 1 1
87.11	8	2 2 0
100.76	11	3 1 0
115.07	4	2 2 2
131.38	18	3 2 1

Table 3.2 Intensities, 2θ values and corresponding planes of nickel collected from 2001 JCPDS.

2θ	INTENSITY	h k l
44.55	100	1 1 1
51.89	42	2 2 0
76.45	21	3 1 1
93.04	20	2 2 2
122.11	7	4 0 0
144.97	14	3 3 1

Fig 3.1 XRD pattern of Ni-30wt% W milled powders at different milling time

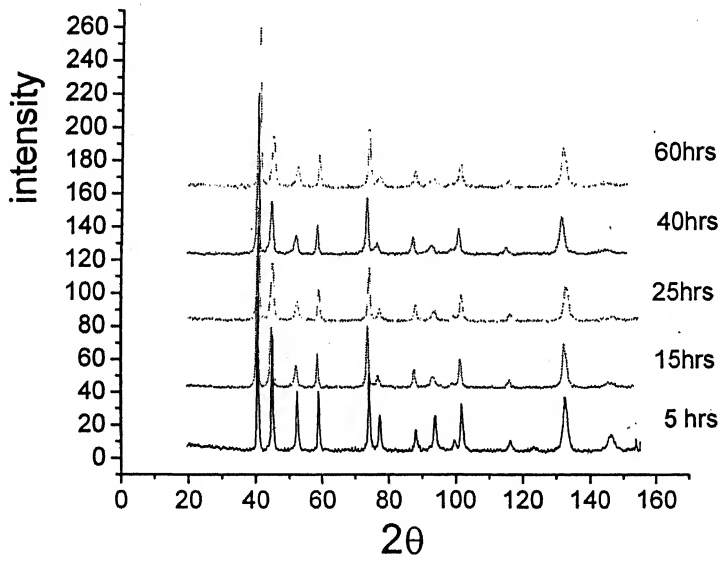

Fig 3.1(a)

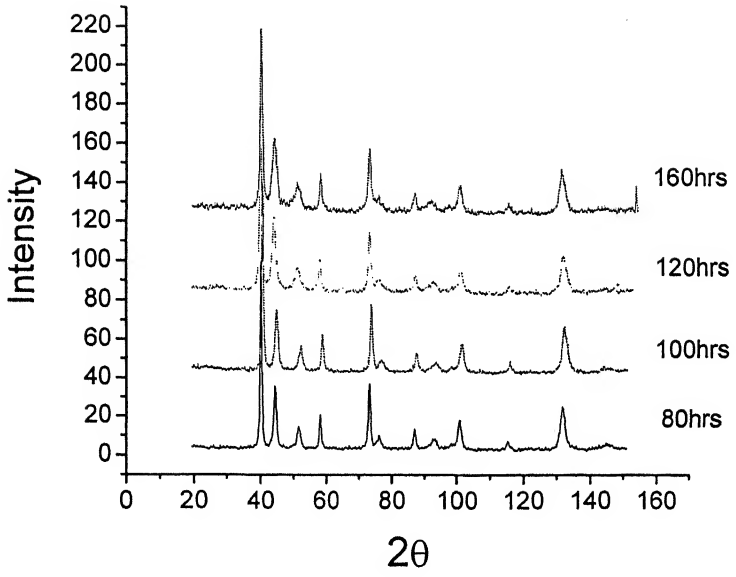

Fig 3.2(b)

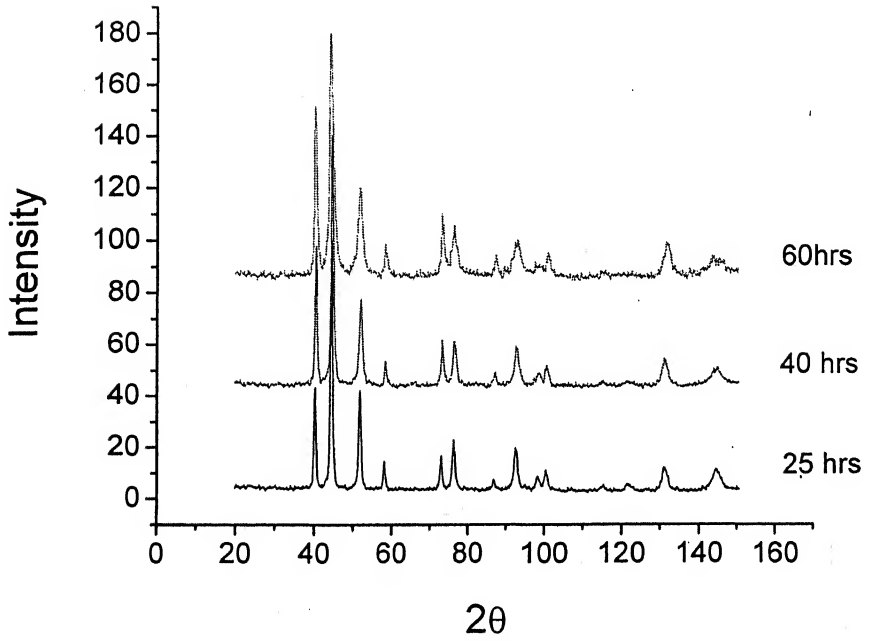

Fig 3.2 XRD pattern of Ni-10wt% W milled powders at different milling time

Table 3.3 Intensities and 2θ values of different peaks of Ni-30wt%W milled for 16 hrs

2θ	INTENSITY
40.33(W)	100
44.26(Ni)	42.89
51.05(Ni)	20.61
58.23(W)	25.06
73.11(W)	16.15
76.13(Ni)	12.22
87.15(W)	19.16
100.89(W)	11.24
115.47(W)	28.99
131.56(W)	20.61

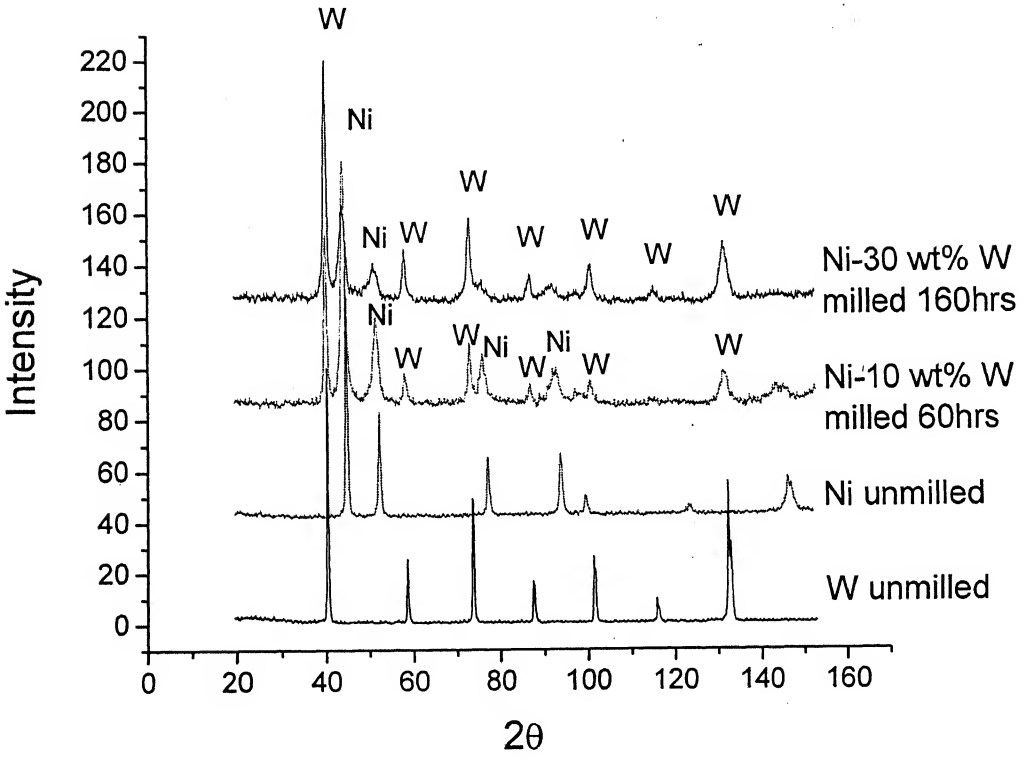

Figure 3.3 Comparison of the pattern of Ni-30wt% W powder milled 160hrs & Ni-10wt%W powder milled 60 hrs with that of pure Ni and W

3.1.2 Effect of Milling Time on the Morphology of Powder Particles

Particle morphology during mechanical milling of ductile powders develops through repeated and intermittent cycles of flattening and impact welding of individual powder particles. Composite particles thus produced get repeatedly

flattened and cold welded and ultimately become severely work hardened. At this stage the particles undergo fracture exposing less work-hardened softer interior to the surface. The repeated flattening - impact welding - fracture of composite powders keeps occurring during milling operation. Mechanical alloying between constituent powders is expected to occur during theses intermittently occurring events.

As already shown by the XRD results, no mechanical alloying occurred in Ni - W powders belonging to 10 wt% and 30 wt% W Ni-W systems for the milling times observed in the present study. The identity of starting Ni and W powder particles was also observed by the powder morphology studies by the scanning electron microscopy (SEM). As shown in Chapter 2, particle morphology of the starting nickel and tungsten powders are shown in Figures 2.1 and 2.2 respectively. It is seen that while nickel powder particles were more or less equiaxed with a mean size of about 150 μm tungsten powder was in the form of a loose agglomerates of more or less equiaxed particles of a mean size of ~ 15 μm.

SEM images of Ni-30wt%W powders milled for 5, 15, 25, 40, 60, 80, 100, 120 and 160 hours of milling time are shown in fig 3.7 to 3.15. Similarly, SEM images of Ni-10 wt% W powders milled for 25, 40 and 60 hours of milling time are shown from Figures 3.16 to 3.18. The structure after a milling time of 5 hours, Figure 3.7, shows both nickel as well as tungsten powder particles in the flaky morphology. Though, as shown in Figures 2.1 and 2.2, there was a considerable difference in the sizes of Ni and W powders, the difference in sizes of flakes of individual Ni and W particles does not appear that big after a milling time of 5 hours. Such an observation suggests that much coarser but ductile nickel particles flatten considerably during early stages of milling and also undergo a severe work hardening. The severe work hardening of them also makes them brittle and therefore prone to fracture. In contrast, hard tungsten particles, due to its higher yield strength, do not undergo very severe plastic deformation and flattening and therefore their work hardening during first five hours of milling remains restricted. Therefore, due to this difference in mechanical properties of nickel and tungsten, while both nickel and tungsten powders do flatten severely deformed nickel particles undergo much more fracture than tungsten particles present in the same stock. Flaky particles of nickel and tungsten with not a very big size difference, as present in the starting powders, therefore are found after the milling time of 5 hours.

With increase in milling time more frequent impact welding of already flattened nickel and tungsten particles occurs. The composite powder particles thus formed continue deforming plastically and undergo their repeated fracture. The embedded flaky tungsten in composite particles thus becomes dispersed an increasingly finer sizes. Clearly identified dispersed W particles embedded in composite powder granules were observed up to the milling time of 100 hours. For milling times of more than 100 hours, the dispersion of W in composite granular particles appears to be extremely fine so as not to be revealed in SEM even at higher magnification. It is worth noting that W dispersoids, though not visible in the SEM images, are present in the material as X-ray diffraction results clearly indicate the presence of elemental W even at this stage. Occurrence of no alloying was also revealed EDS from individual particles [Figures 3.19 and 3.20].

3.1.3 Particle Size Refinement of Ni-W Powders during Milling

It has been already been discussed that the milling of Ni-W powders corresponding to Ni-10 wt% W and Ni-30 wt% W powders did not produce mechanical alloying up to the milling time intervals observed in the present study. Further, morphological studies by the SEM showed that the milled powder contained dispersion of W. As the milling time increased the dispersion of W became finer and finer. The present section shows the results obtained regarding the particle size distribution of milled Ni-W powders as function of milling time.

It is seen that for Ni-30 wt% W powder, during 0-5 hrs of milling, the mean particle size is 35.4 μm, which decreases rapidly to 4.3 μm with increase in milling time to 15 hrs and thereafter till 160 hrs of milling the mean size remains steady between 4-6 μm. Initial ball- powder- ball collision causes particles to cold weld giving larger particle size as seen from 0-5 hrs of which get reduced with fracture only after sufficient work hardening of individual particles has occurred With increased milling time, fracture within individual particles is pronounced leading to mean particle size of 4.3 μm after 15 hrs of milling. However from the particle size distribution curve it is seen that the range of particle size distribution is wide till 80 hrs of milling after which it narrows down between 2-9 μm and thereafter remains near constant.

Analysis of Ni-10 wt% W shows mean particle size of 30.9 μm and 9.2 μm after 25 and 40 hrs of milling. Both the values are higher when compared to the particle size of Ni- 30 wt% W powder at same milling times. This can be explained, since W being brittle and work hardens heavily during mechanical deformation leading to fracture, a higher% of W in Ni- 30 wt% W powder made the system more brittle. So the amount of work hardening require for fracture of individual particles is reached much early in Ni- 30 wt% W powder leading to smaller mean particle size after a short milling time of 5 hrs.

3.1.4 Reduction of the Crystallite Size during Milling

The XRD patterns of both Ni-10wt%W and Ni-30wt%W milled powders revealed broadening of peaks with increase of milling time. Such observation confirms that crystallite size of the milled powder gets decrease as the milling time increases. Crystallite size was analyzed by studying the broadening at half of the maximum intense peak in the XRD pattern. However, broadening can also occur due to instrumental error. This broadening was taken care by taking XRD pattern of standard Si sample and eliminated the FWHM value (of the peak at same position as in our sample under investigation) of standard Si sample from the FWHM value of sample under investigation.

The effect of milling time on the crystallite size of Ni and W in the milled powders is shown in Figures 3.4 & 3.5. It is observed that in Ni-30 wt% W milled powder there was a rapid decrease in the crystallite size of Ni till 60 hrs and then again from 100 to 160 hrs of milling; whereas in between 60 &100 hrs of milling the decrease in crystallite size was found to be less rapid. A rapid decrease in the crystallite size of Ni was also observed in the case of Ni-10 wt% W milled powder. The reason for this trend is that in the initial phase of milling powder particles are deformed and fractured severely which causes accumulation of defects, dislocations, stacking faults etc. and these features cause severe distortions in the lattice. These defects become localized in the shear bands formed and then disintegrate into small grains due to higher instability of the structure as milling time is increased beyond 100hrs. The crystallite size of W in both the powders shows a much slower rate of decrease with milling time compared to Ni.

Table 3.4 Crystallite size of Ni & W in Ni-30wt%W milled powder at different Milling times

Milling time (hrs)	**Crystallite size(nm)**	
	Ni	W
5	14.19	11.88
15	11.20	11.05
25	8.16	10.56
40	6.95	9.56
60	5.87	9.11
80	5.26	8.72
100	4.98	8.23
120	3.74	7.90
160	2.41	7.36

Table 3.5 Crystallite size of Ni & W in Ni-10wt%W milled powder at different Milling time

Milling time (hrs)	**Crystallite size(nm)**	
	Ni	W
25	11.78	9.80
40	9.33	9.12
60	6.88	8.73

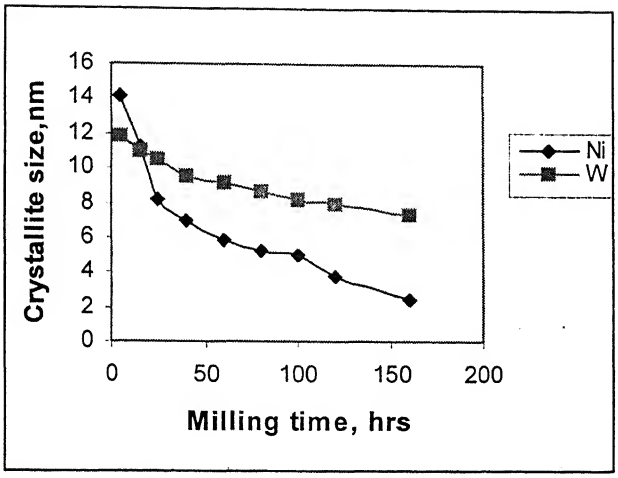

Fig 3.4 Effect of milling time on crystallite size of Ni and W particles in Ni- 30 wt% W powder

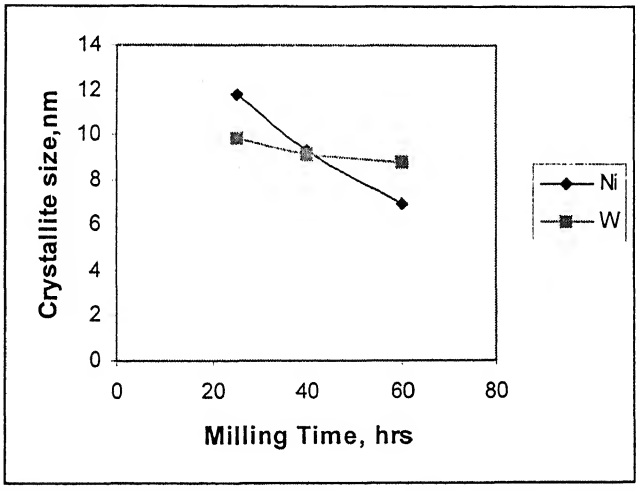

Fig 3.5 Effect of milling time on crystallite size of Ni and W particles in Ni- 10 wt%W powder

.

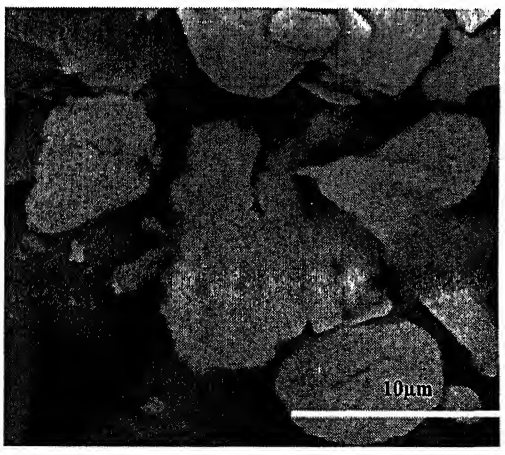

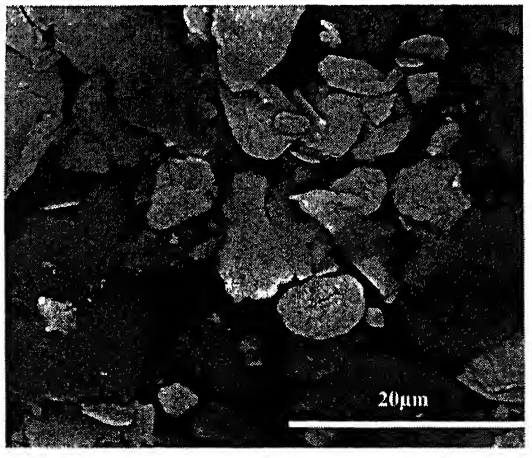

Fig 3.6 & 3.7 Ni- 30 wt% W powder milled 5 hrs

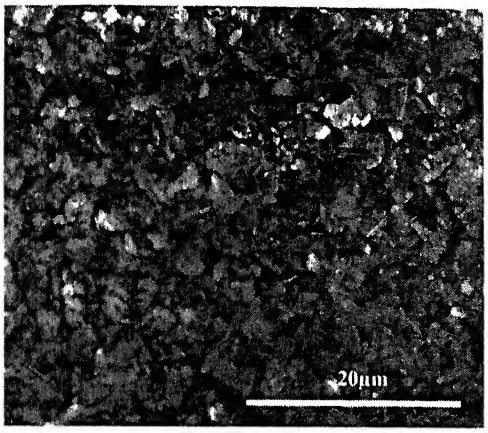

Fig 3.8 Ni- 30 wt% W powder milled 15 hrs

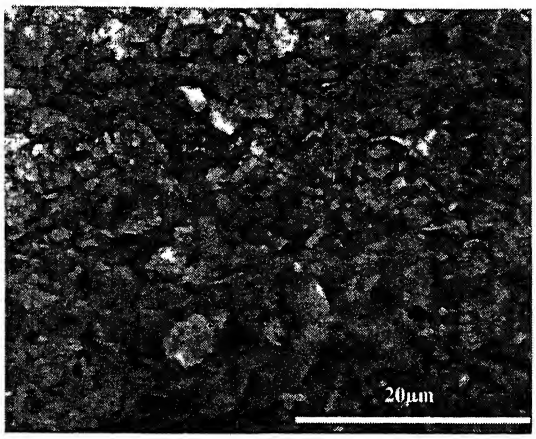

Fig 3.9 Ni- 30 wt% W powders milled 25 hrs

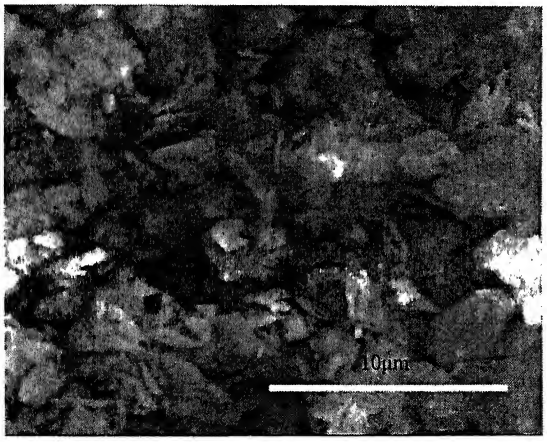

Fig 3.10 Ni- 30 wt% W powder milled 40 hrs

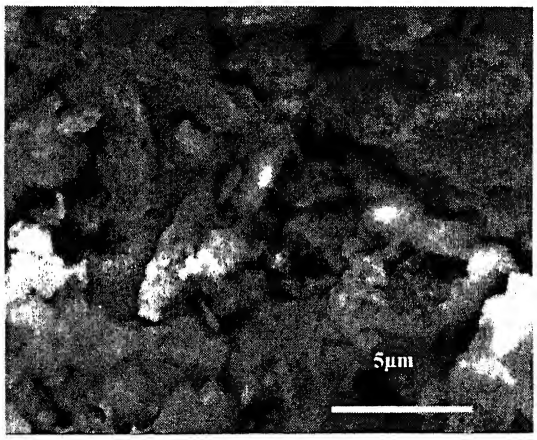

Fig 3.11 Ni- 30 wt% W powder milled 60 hrs

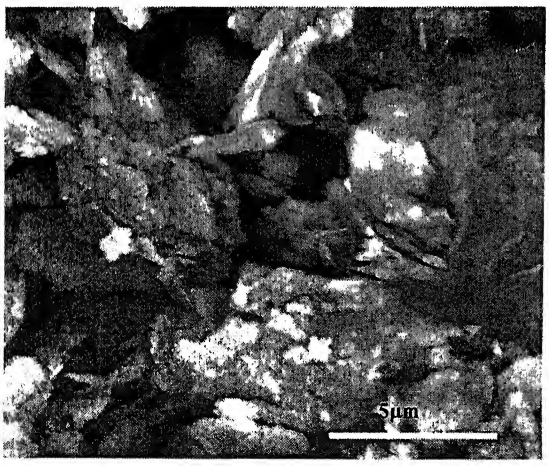

Fig 3.12 Ni- 30 wt% W powder milled 80 hrs

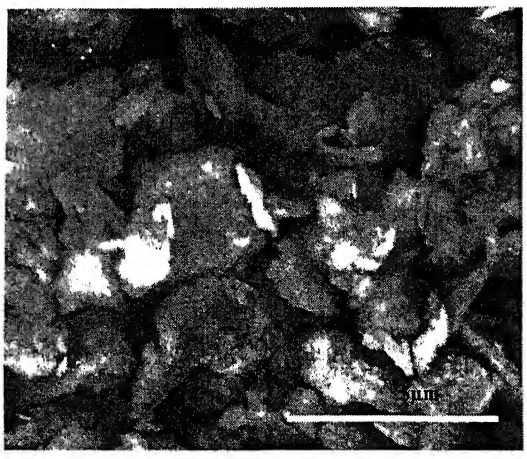

Fig 3.13 Ni- 30 wt% W powder milled 100 hrs

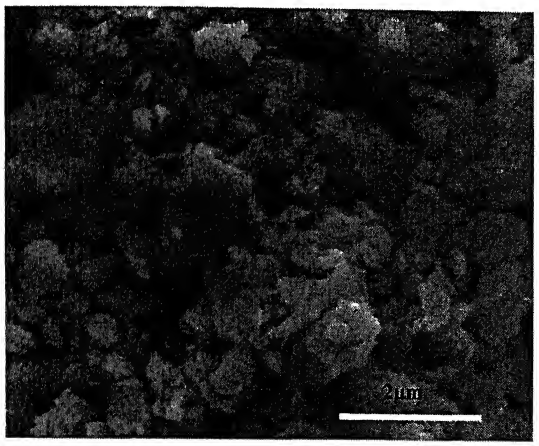

Fig 3.14 Ni- 30 wt% W powder milled 120 hrs

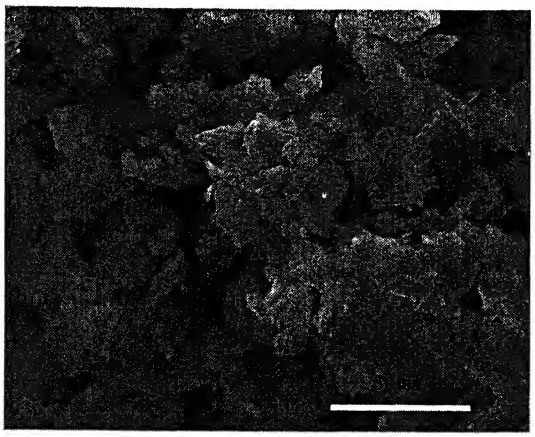

Fig 3.15 Ni- 30 wt% W powder milled 160 hrs

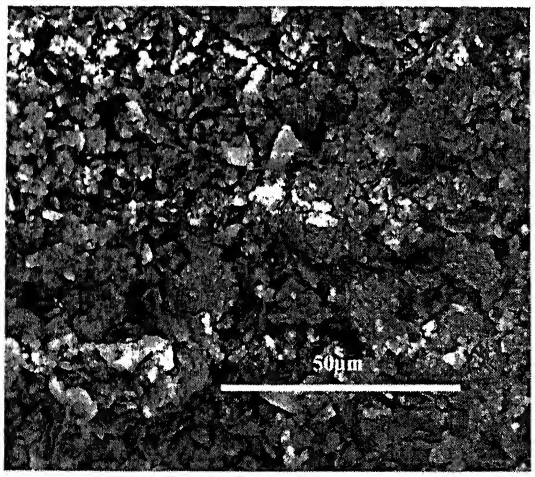

Fig 3.16 Ni- 10 wt% W powder milled 25 hrs

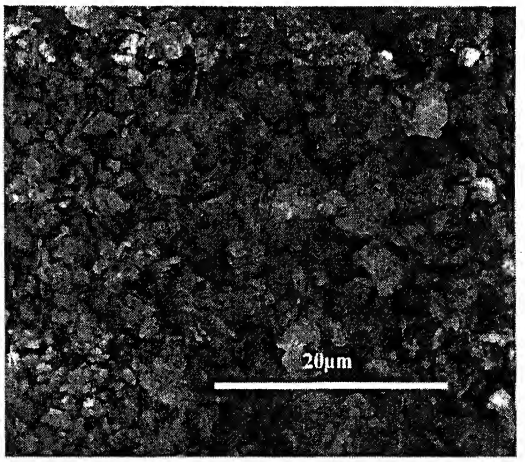

Fig 3.17 Ni- 10 wt% W powder milled 40 hrs

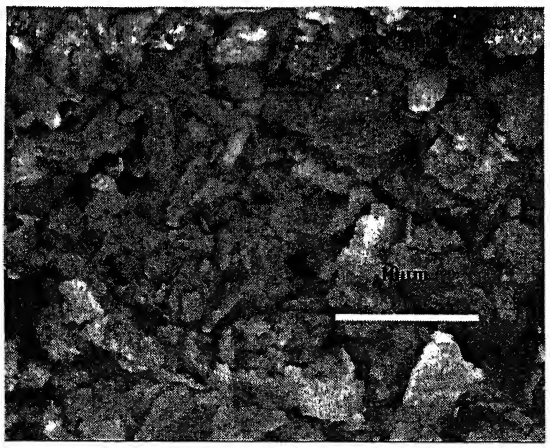

Fig 3.18 Ni- 10 wt% W powder milled 60 hrs

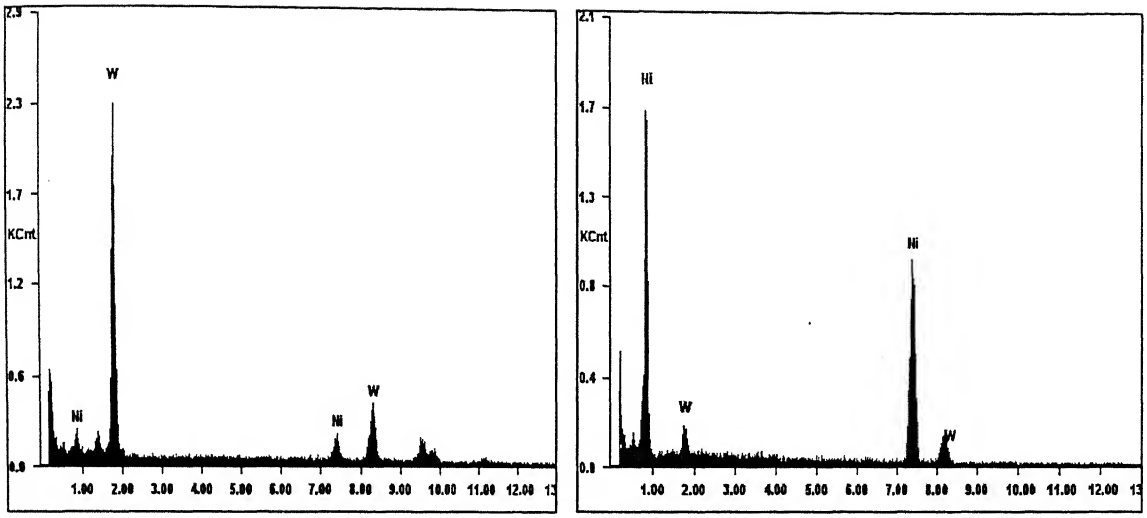

EDS – W particle EDS- Ni particle

Fig 3.19 EDS from W & Ni particles of Ni-30wt% W powder milled 40 hrs

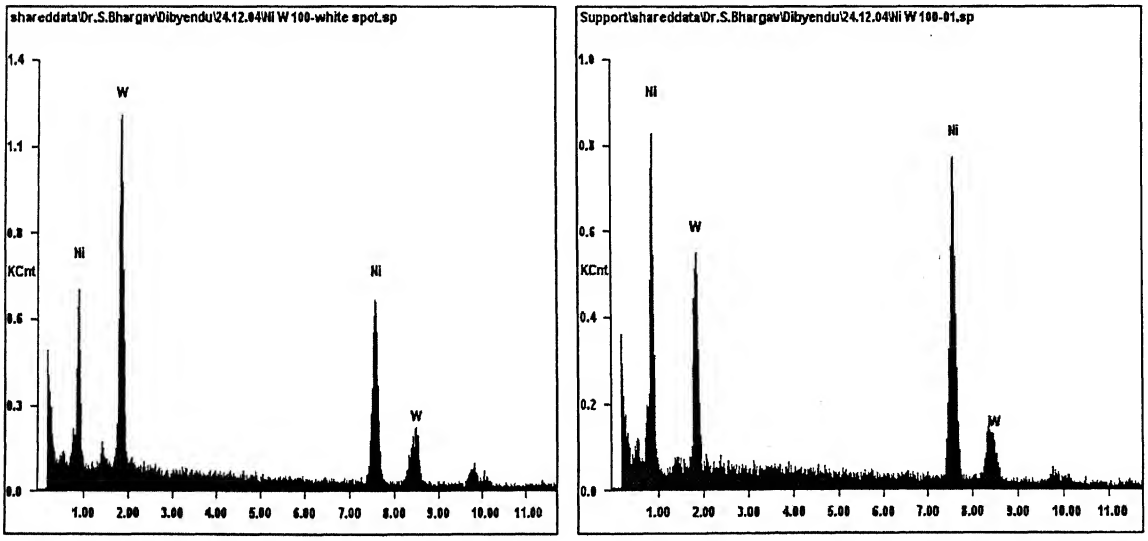

EDS – W particle EDS- Ni particle

Fig 3.20 EDS from W & Ni particles of Ni-30wt% W powder milled 100 hrs

Particle size distribution of Ni-30wt% W milled 5 hrs

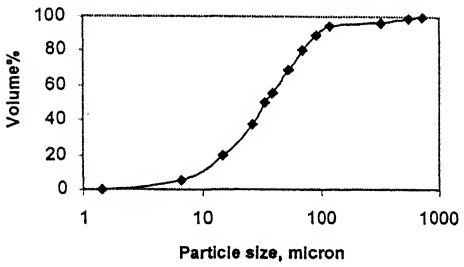

Particle size distribution of Ni-30wt% W milled 15 hrs

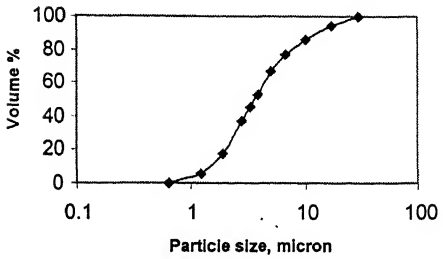

Particle size distribution of Ni-30wt%W milled 25hrs

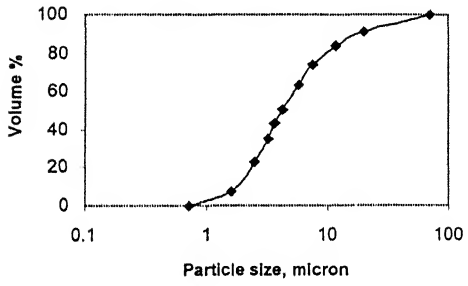

Particle size distribution of Ni-30wt%W milled 40 hrs

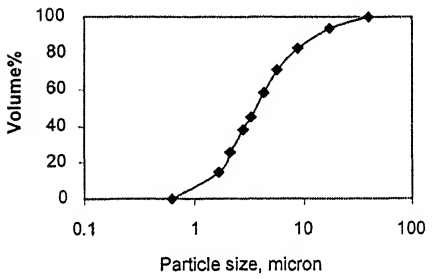

Particle size distribution of Ni-30wt% W milled 60 hrs

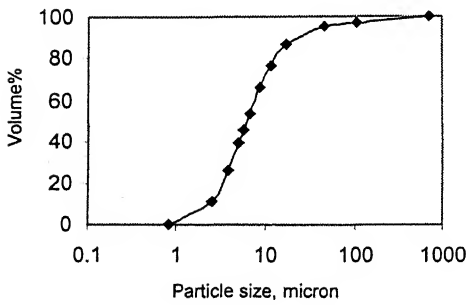

Particle size distribution of Ni-30 wt% W milled 80 hrs

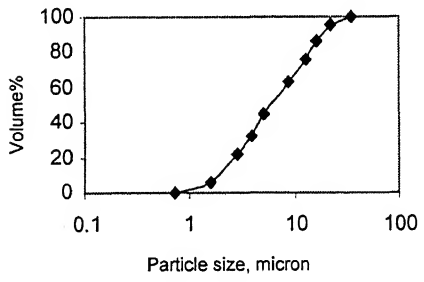

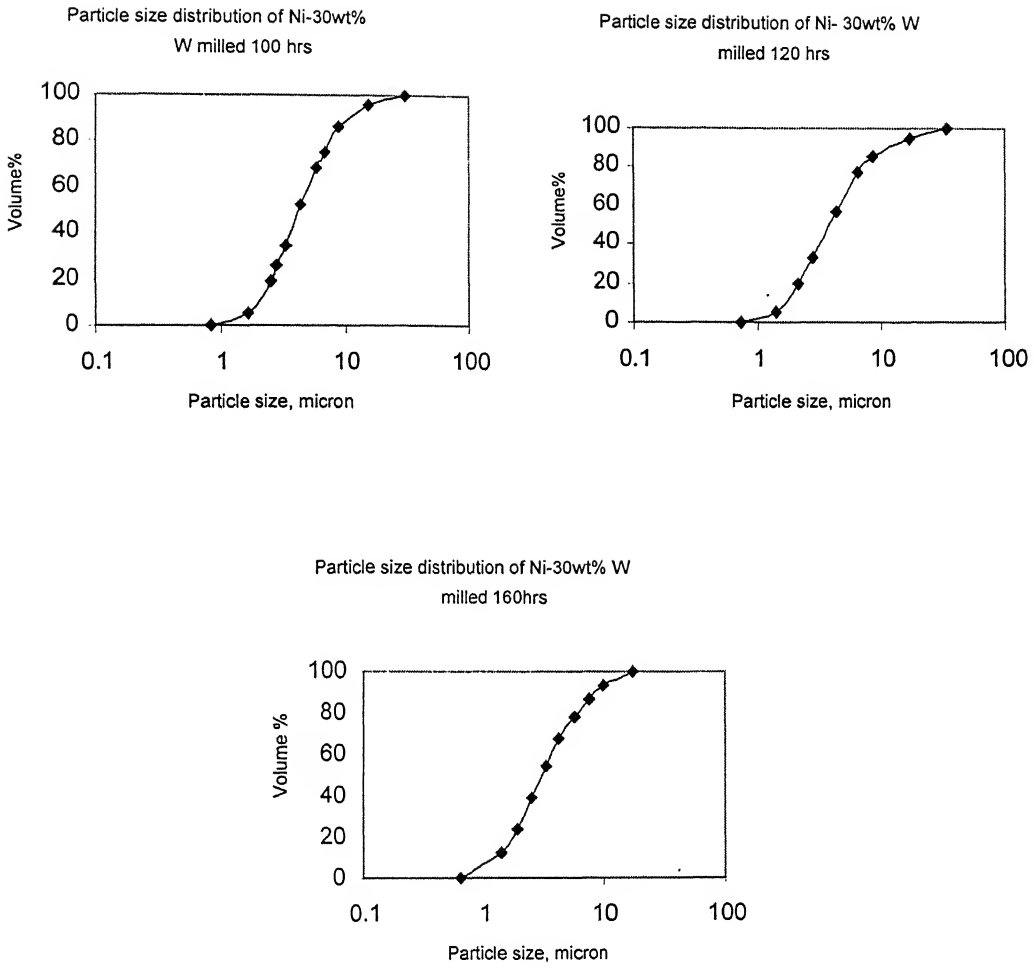

Fig 3.21 Particle size distribution of Ni-30wt% W powder at different milling times

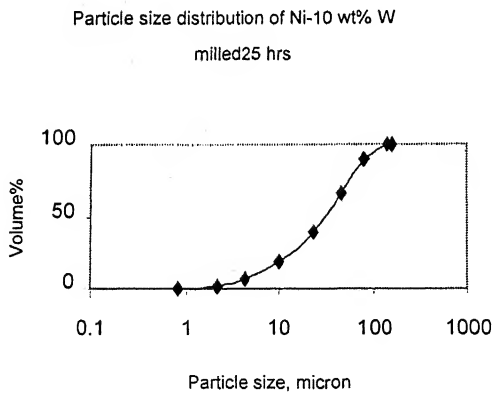

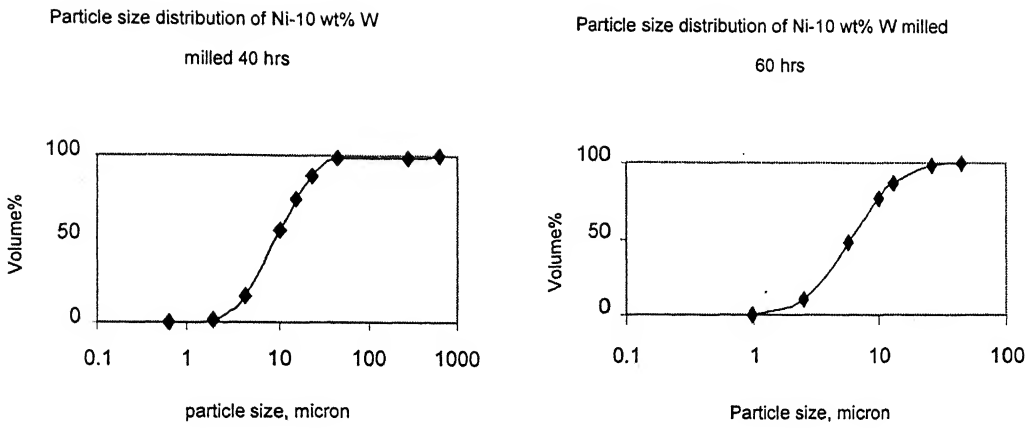

Fig 3.22 Particle size distribution of Ni-10wt% W powder at different milling times

3.2 SINTERING OF STRIPS

Prior to their densification rolling by cold rolling - sintering route, single layered Ni-W and bi-layered Ni - Ni-W compacted strips were sintered at 900°C for 90 mins under protective atmosphere. True density of sintered strips was calculated using Archimedes principle, the procedure for which been described in the previous chapter. Table 3.6(a) shows the densities of the strips after their sintering. Since the amount of tungsten varied in single-layered and bi-layered strips, the theoretical densities of different strips was calculated using weighted law of addition. This method of density calculation makes a reasonable assumption because, as revealed by the X-ray diffraction results, milling of Ni and W powders did not produce any solid solution between Ni and W. Theoretical densities of different single-layered and bi-layered strips is shown in Table 3.6 (b). Relative densities of different strips were then calculated using the values of their theoretical densities.

Table 3.6(a) Density of sintered strips

Material	Strip I	Strip II	Strip III	Strip IV	Strip V	Strip VI
Density of Sintered Strips, 10^3 Kgm^{-3}	7.36	5.4	6.21	6.4	9.25	7.43
Relative Density	74%	58%	66%	68%	77%	71%

Table 3.6(b) Theoretical Density of strips

Material	Single layer Ni-10 wt% W	Bilayered Ni- 10 wt% W & unmilled Ni	Single layer Ni- 30 wt% W	Bilayered Ni-30 wt% W & unmilled Ni
Theoretical density of different Ni-W strips, (10^3 Kg.m^{-3})	9.94	9.6	12.01	10.46

Strip I: Single layer; Ni- 10 wt% W- milled 60 hrs
Strip II: Bilayered; Ni- 10 wt% W- milled 25 hrs + unmilled Ni

Strip III: Bilayered; Ni- 10 wt% W- milled 40 hrs + unmilled Ni
Strip IV: Bilayered; Ni- 10 wt% W- milled 60 hrs + unmilled Ni
Strip V: Single layer, Ni- 30 wt% W- milled 60 hrs
Strip VI: Bilayered, Ni- 30 wt% W- milled 60 hrs + unmilled Ni

It is seen from tables 3.6(a) & (b), density in the sintered strips is only 65-75% of the theoretical densities. It indicates that proper densification is not achieved during sintering. The trend in the density values of sintered strips have been summarized in figs 3.23 & 3.24. It is seen that the density of sintered bilayered strips having same compositions and sintering conditions increases with increase in milling time of the Ni-W powder. Since powders milled for longer time have a finer grain size and hence more surface area, the surface free energy term acting as the driving force for sintering becomes higher for such powders resulting in better densification.

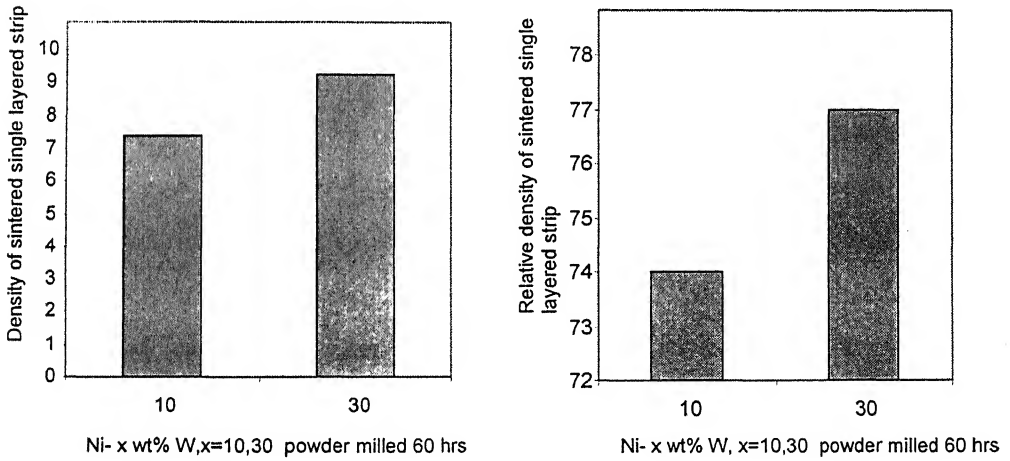

Fig 3.23 Variation of density of single layered strips with composition

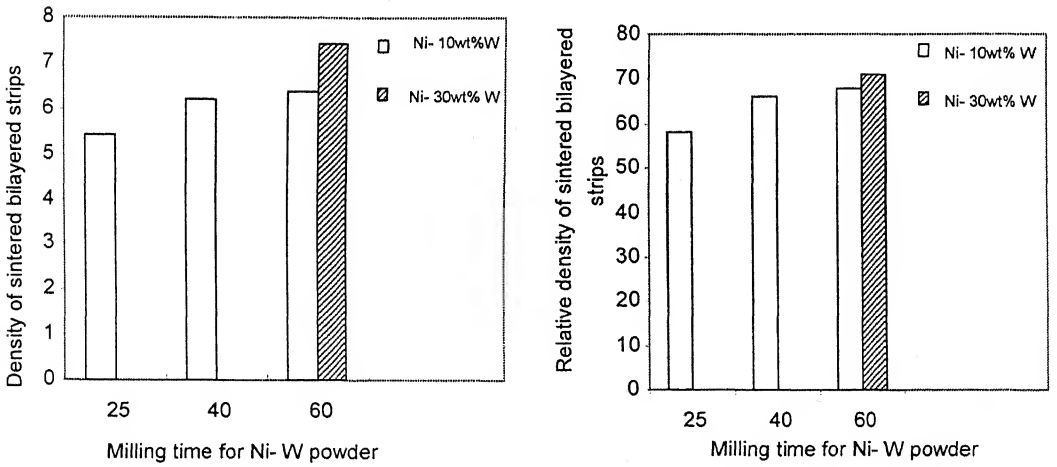

Fig 3.24 Variation of density of bilayered strips with milling time

It is also observed that with the milling time being the same the density of both single-layered Ni-W and bi-layered Ni - Ni-W strips increases with increasing the wt% of W. It must be noted that there are three types of interfaces present in the system: Ni-Ni, Ni-W and W-W. It has been shown that after sufficient milling W particles are uniformly dispersed and got embedded on Ni. So it can be assumed that W-W interfaces become negligibly small after a milling time of 60 hrs and only Ni-Ni and Ni-W interfaces are predominantly present in the system. With an increased wt % of W in the system the Ni-W interfaces become more and since Ni-Ni and Ni-W interfaces have different interfacial energies a difference in sintering kinetics in Ni-W systems of different compositions is expected. Though the values of interfacial Ni-Ni and Ni-W energies are not readily available, it appears from the results obtained in the present study that a higher Ni-W interfacial area promotes faster sintering kinetics. This difference in different Ni-W systems can perhaps be used to explain the higher sintered relative densities achieved in systems containing higher W.

Fig 3.25 shows the three-dimensional images of the bi-layered Ni - Ni-30 wt % W sintered strips. It can be seen that a concave curvature developed towards the Ni-W layer in all the sintered bi-layered strips due to differential shrinkage occurring in individual layers. It is to be noted that the individual layers of the bi-layered strips were prepared by compacting unmilled Ni powder and milled Ni-W powder. Since the sintering was done at 900°C, i.e. at 0.68 T_M of nickel, the sintering kinetics of pure nickel layer made up of unmilled nickel powder was not expected to be very high. In contrast, due to the nano-crystalline grain size existing in the milled Ni-W powder layer the sintering kinetics becomes considerably fast even at the low sintering temperature. It is worth noting the surface free energy term that acts as the driving force for sintering becomes much higher for nanocrystalline milled Ni-W powders. Besides various mass transport mechanisms, like grain boundary diffusion, responsible for sintering exhibit particle size dependence since the very fine size of grains becomes comparable to the characteristic length for transfer process. Hence, kinetics of the atomic process involved in densification was also enhanced. Thus, compared to that occurring in pure Ni layer, much higher sintering rates occurred in Ni-W layers in all the bi-layered compacts. It was further observed that the concave

curvature developed in bi-layered strips decreased with increasing the milling time for all the sample.

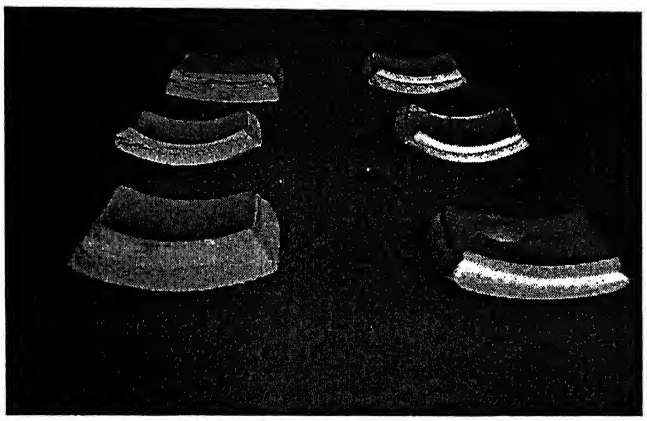

Fig: 3.25 Digital images of strips after sintering

Since the sintered bi-layered Ni - Ni-W strips were prepared for the purpose of their subsequent densification by a suitable cold rolling - annealing route, the degree of flatness of the bi-layered strips was among the major concerns for fixing the milling and sintering parameters. It is to be noted that while increasing the milling time increases the extent of fine dispersion of W in Ni, it also increases the sinterability of the powder which, in turn, causes a concave curvature to the sintered bi-layered strips and hence affects their flatness. The milling of Ni-W powders for further work was therefore restricted to 60 hrs and both single-layered Ni-W strips and bi-layered Ni - Ni-W strips were prepared from powders milled up to 60 hours only

3.3 Densification Rolling of Sintered Strips

It has been reported by many researches that fully dense strip can be made from sintered strip by a series of cold rolling and sintering/ annealing cycles. Single and bilayered sintered strips, made from Ni-10wt% W milled for 25, 40, & 60 hrs and unmilled Ni, having densities in the range of 65-75% of theoretical values, were subjected to 3-4 cycles of cold rolling and sintering/annealing. In each cycle single-layered Ni-10 wt% W or Ni-30 wt% W and bi-layered Ni - Ni-10 wt% W strips were cold rolled to a thickness reduction of 35 - 50% and were subsequently annealed at 900°C for 30 minutes.

Table 3.7 Typical cold rolling & annealing cycle for densification of sintered strips

Material	Density of Sintered Strips. 10^3 $Kg.m^{-3}$	Cold Rolling Thickness red^n %	Annealing Parameters Temp,K; Time,min; Atm	Cold Rolling Thickness red^n %	Annealing Parameters Temp,K; Time,min; Atm	Cold Rolling Thickness red^n %	Annealing Parameters Temp,K; Time,min; Atm	Cold Rolling Thickness red^n %	Total Cold Rolling Thickness red^n %	Density of Sintered Strips, 10^3 $Kg.m^{-3}$	Relative density
Strip I	7.36 (74% ρ_{th})	49	1173 30 H_2	37	1173 30 H_2	50	1173 30 H_2	38	89	9.8	98.5%
Strip II	5.4 (58% ρ_{th})	38	1173 30 H_2	51	1173 30 H_2	42	1173 30 H_2		82	9.33	96.8%
Strip III	6.21 (66% ρ_{th})	35	1173 30 H_2	42	1173 30 H_2	40	1173 30 H_2		78	9.26	96.1%
Strip IV	6.4 (68% ρ_{th})	30	1173 30 H_2	34	1173 30 H_2	32	1173 30 H_2		71	9.35	97%

Strip I: Single layer; Ni- 10 wt% W- milled 60 hrs
Strip II: Bilayered; Ni- 10 wt% W- milled 25 hrs + unmilled Ni
Strip III: Bilayered; Ni- 10 wt% W- milled 40 hrs + unmilled Ni
Strip IV: Bilayered; Ni- 10 wt% W- milled 60 hrs + unmilled Ni

Table 3.7 shows the density of the strips after final roll pass. It is seen that final rolled strips obtained relative densities in the range of 96-98% of the theoretical density.

Fig 3.26 and 3.27 show the typical microstructure of rolled bi-layered Ni - Ni-10 wt% W strips prepared from the unmilled nickel powder and Ni-W powder milled for 40 hours after first two cold rolling-annealing cycles. Similar microstructural features were observed in strips prepared from Ni-W powders milled for 20 and 60 hours respectively. Some large elongated pores are seen in the structure after first roll pass. Smaller pores are also visible. However the Ni layer seems to be more porous than the Ni-W layer. This is evident as densification of the Ni-W layer was more during sintering than Ni layer which also resulted in curvature of the strips as discussed earlier. It is also noted that lesser pores are seen in the structure after second roll pass. This is due to the fact that some pores got welded up during rolling. The white region in Ni-W layer is W rich phase and the dark region is Ni. This is also supported by the microhardness values taken from the individual regions in the Ni-W layer.

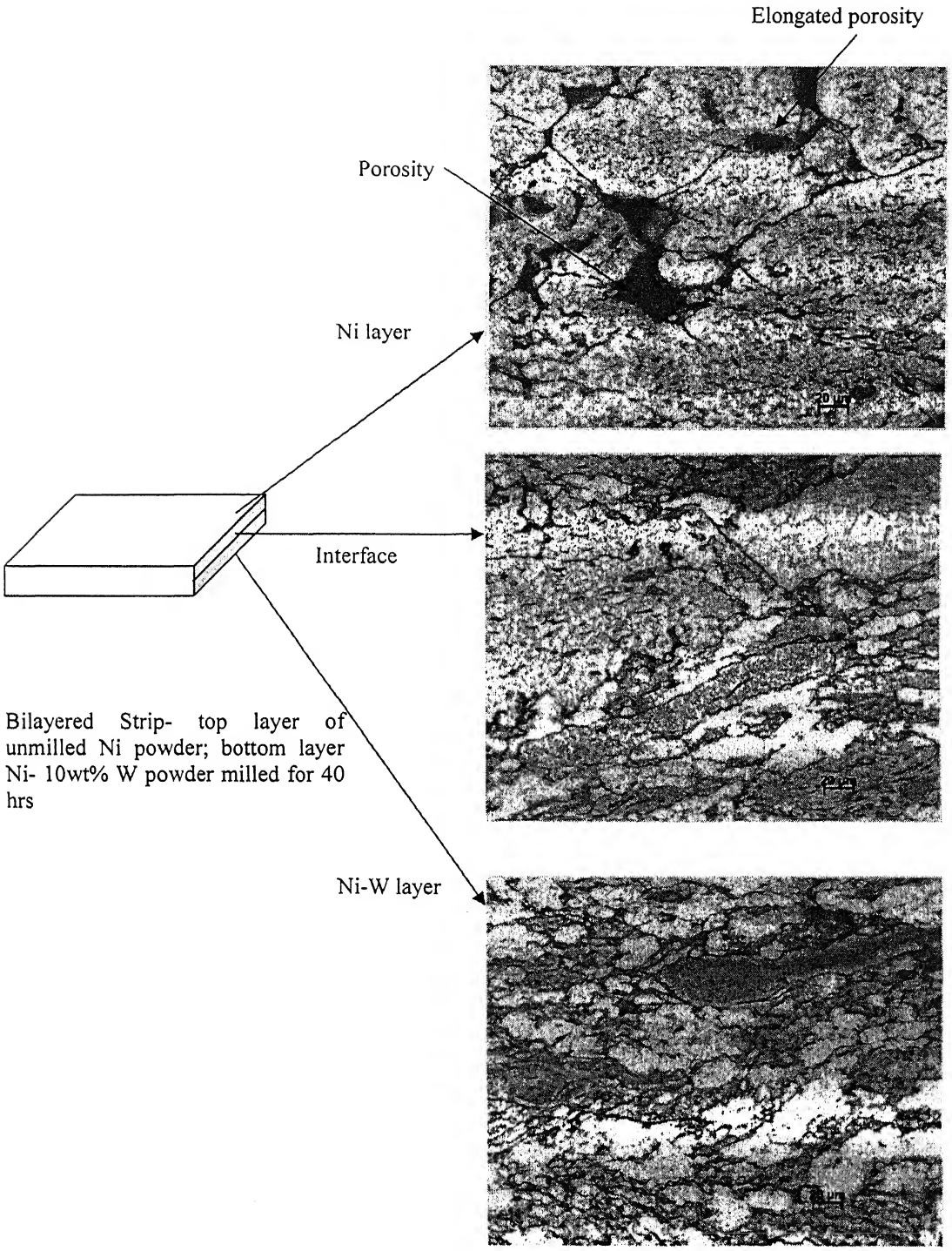

Fig 3.26 Optical micrographs of a bilayered strip after first roll pass

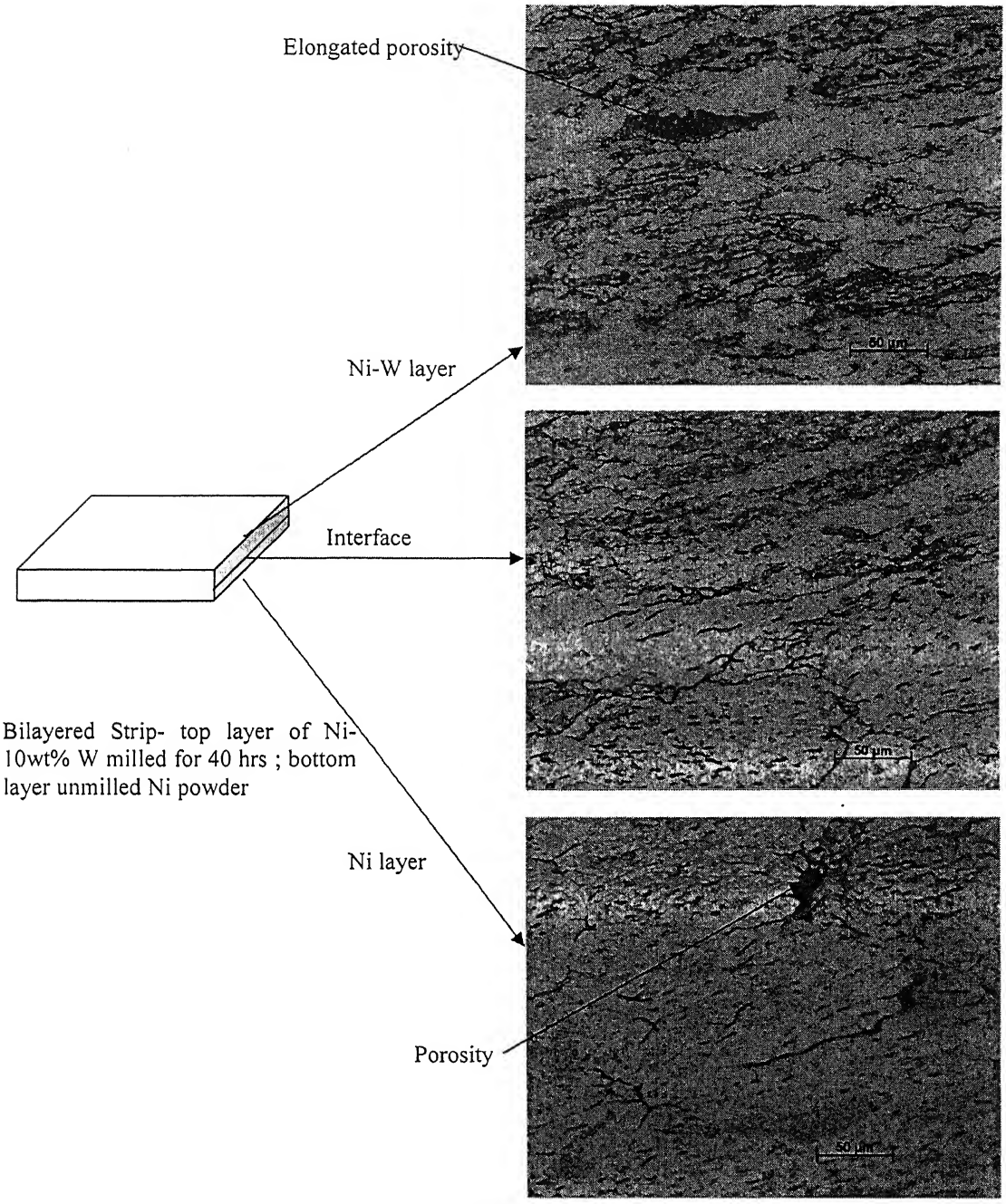

Fig 3.27 Optical micrographs of a bilayered strip after second roll pass

3.4 Mechanical Properties of Rolled Strips

3.4.1 Microhardness Results

Table 3.8 shows the microhardness values, of both single and bilayered strips, after each cold rolling pass. The hardness values of the rolled strips are higher compared to pure Ni which is around 600Kg\mm^2. This is primarily due to strain hardening of the material on cold working. Increase in hardness value is seen after successive roll passes though intermediate annealing is done. The reason behind this is that the soaking time at the annealing temperature (1173K) was not sufficient for complete recrystallisation and removal of internal strain and that lead to a more strain hardened structure after each roll and increased hardness values.

Table: 3.8 Vickers Microhardness Values, HV (Kgf\mm^2) of Rolled Strips

Specimen Cold Rolling Pass	Single Layer strip (Ni-10wt%W-milled 60hrs)	Bilayered strip (Ni-10wt%W-milled 25 hrs & unmilled Ni)	Bilayered strip (Ni-10wt%W-milled 40 hrs & unmilled Ni)
I	815 940	675 802 960	689 861 974
II	882 1026	724 853 1144	841 890 1027
III	890 1083	788 1027 1362	883 1125 1246
IV	1064 1284	-	-

3.4.2 Tensile Properties

Table 3.9 shows results of tensile tests performed on dog bone samples obtained from single and bilayered rolled strips. The trend in the yield strength and tensile strength values of the samples have been summarized in fig 3.28 and 3.29. It is seen that both yield and tensile strength is increased with increase in milling time. Tensile tests reveal a yield strength of the rolled strips which is a factor of 12-15 higher than that of pure Ni. The ultimate tensile stress of rolled strips is a factor of 3 higher compared to that of 215 MPa for pure Ni. The ultimate tensile strength is reached at a plastic strain of about 1% only .This is expected due to high strain hardening of the strips as a result of heavy cold working. This reason holds good for the very low %elongation of the strips of about 1-1.5%. However, since the superconductive does not withstand a strain above 0.2% in tension without degradation, more important for the application of substrate is the stress at low strains which is measured at an irreversible strain of 0.2%. The rolled strips start to deform

plastically at stress level above 550MPa. In comparison the pure Ni tape has yield strength of only 48MPa. The primary mechanism by which the improvement in the mechanical properties occurs is believed to be the strengthening due to cold working.

Table 3.9 Tensile Properties parallel to the rolling direction

	Bilayered strip (Ni-10wt%W- milled 25 hrs & unmilled Ni)	Bilayered strip (Ni-10wt%W- milled 40 hrs & unmilled Ni)	Single Layer strip (Ni-10wt%W- milled 60hrs)
Yield strength MPa	560	622	728
UTS MPa	622.796	687.876	795.88
% elongation	1.33	1.49	1.41

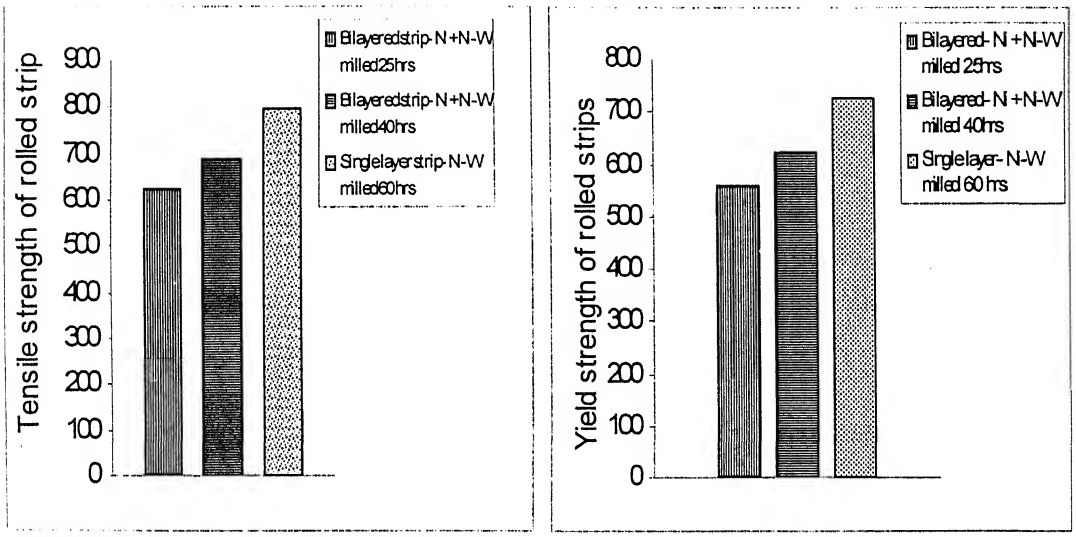

Fig 3.28 Yield and tensile strength of different rolled strips

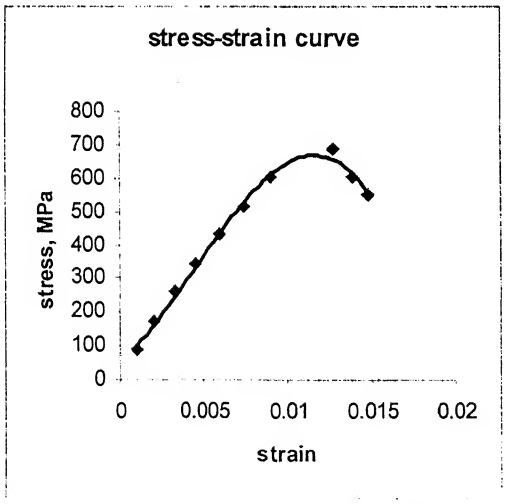

Fig 3.29 Engg. Stress-Strain Curve of Bilayered strip (Ni-10wt%W- milled 40 hrs & unmilled Ni)

3.5 Fractography

Fig 3.30-3.32 shows the SEM images of the fracture surfaces of the tensile test samples which were made from the rolled strips. The fracture is produced by a single application of uniaxial tensile stress. A careful examination of the fracture surfaces reveals the presence of predominantly cleavage and also dimple rupture modes of fracture.

Cleavage fracture represents brittle fracture and is characterized by the presence of flat facets; usually the flat facets exhibit river markings. SEM images of the fracture surfaces show the presence of such river markings. The river markings are caused by cracks moving through the crystal along a number of parallel planes which form a series of plateaus and connecting ledges. These are indications of absorption of energy by local deformation. The direction of river pattern is the direction of crack propagation. The presence of brittle mode of fracture can be explained by the fact that the strips were subjected to heavy plastic deformation to produce dislocation pile-ups, microcracks are generated due to buildup of shear stress at the head of pile-ups and eventually propagation of microcracks occurs when stress level reaches the fracture stress. Presence of elastic stored energy due to prior deformation influences the crack propagation to occur at lower stress level.

Presence of dimple rupture mode of fracture is also evident from the cup like depressions formed on the fracture surfaces. The cup- like depressions are caused by mechanism of microvoids initiation at second phase- W, voids growth and eventually fracture of ligaments between the microvoids.

SEM Images of Fracture Surfaces

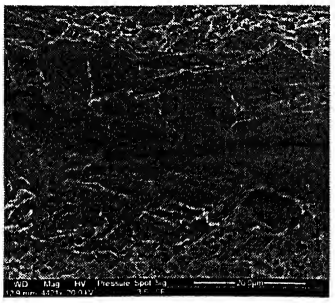

Fig 3.30 Bilayered strip (Ni-10wt%W- Milled 25 hrs & unmilled Ni)

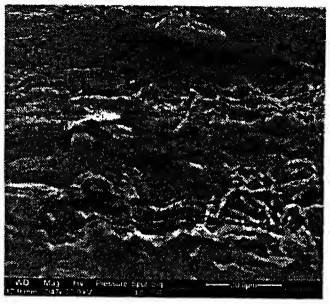

Fig 3.31 Bilayered strip (Ni-10wt%W- Milled 40 hrs & unmilled Ni)

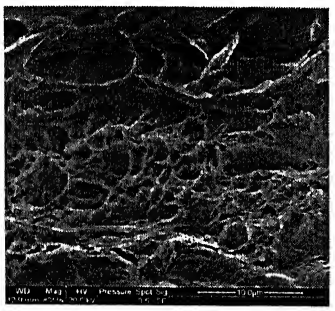

Fig 3.32 a

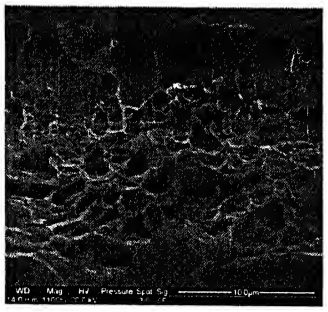

Fig 3.32 b

Single Layered Strip (Ni-10wt%W- milled 60 hrs)

CONCLUSIONS

The following conclusions can be drawn from the results of the present study:

1. As determined by X – ray diffraction method Ni and W exits in the final milled powder in elemental form; no new phase-due to alloying, oxidation or contamination is formed. The crystallite size of Ni-10 wt% W and Ni-30 wt% W decreases with milling time. There is a rapid decrease in the crystallite size till 60 hrs of milling and then again from 100 to 160 hrs of milling; in between 60 &100 hrs of milling the decrease in crystallite size is less rapid

2. As reveled by the scanning electron microscopy, particle morphology of mechanically milled Ni–10 wt% W and Ni–30 wt% W powders changes with increase in milling time. The particle morphology changes from spheroidal to irregular as the milling time increases. With increasing milling time, the W particles become finer and get uniformly distributed in particles of Ni. After a milling time of 160 hrs, the distribution of W particles becomes so fine that their separate presence is not readily observed in powders even at very high magnification under the SEM. However no alloying occurs as revealed by EDS from individual particle.

3. In the Ni-30 wt% W powder, during 0-5 hrs of milling, the mean particle size is 35.4 μm, whereas the mean particle size of unmilled Ni is 152 μm and that for unmilled W is 17μm. So there is a rapid decrease of Ni particle size within only 5 hrs of milling. This is due to the fact that Ni particles being ductile can be deformed easily, so deformation within Ni particles is more leading to work hardening of the particles till eventually fracture occurs. From 5 to 15 hrs of milling the mean particle size decreases rapidly to 4.3 μm and thereafter tills 160 hrs of milling the mean size remains steady between 4-6 μm.

4. At the sintering temperature of 900°C (0.67 of T_M of Ni) a high sintering rate and better densification is observed for Ni-W milled powder compared to unmilled Ni powder in the bilayered strips. This high sintering rate leads to concave curvature

in the bi-layered strips towards Ni-W layer. Density of the sintered bi-layered strips of the same composition and sintering conditions increases with increase in milling time of the powder. Also density increases with W wt% in both single and bilayered strips when milling time is kept the same.

5. Cycles of rolling followed by annealing leads to improved densification of the strips; porosity in both Ni and Ni-W layer gets reduced with cycles of rolling and intermediate annealing resulting in a densified final structure with about <5% porosity.

6. Yield strength of the rolled bi-layered Ni – Ni- 10 wt% W strips is 12-15 higher than that of pure Ni. The ultimate tensile stress of rolled strips is ~ 3 times higher compared to that of 215 MPa for pure Ni. The ultimate tensile strength is reached at a plastic strain of about 1% only. This is expected due to high strain hardening of the strips as a result of heavy cold working. This reason holds good for the very low % elongation which is about 1-1.5%. Also both yield and tensile strengths of the strips are increased with increase in milling time.

REFERENCES

1. A. Goyal, D. P. Norton, J. D. Budai, M. Paranthaman, E. D. Specht, D. M. Kroeger, D. K. Christen, Q. He, B. Saffian, F. A. List, D. F. Lee, P. M. Martin, C. E. Klabunde, E. Hartfield, and V. K. Sikka, "High critical current density superconducting tapes by epitaxial deposition of $YBa_2Cu_3O_x$ thick films on biaxially textured metals", *App. Phy. Lett.*, Vol. 69, No. 12, pp. 1795-1797.
2. B. De Boer, J. Eickmeyer, N. Reger, L. Fernandez G.-R, J. Richter, B. Holzapfel, L. Schultz, W. Prusseit and P. Berberich, "Cube textured Nickel Alloy Substrates for $YBa_2Cu_3O_{7-\delta}$-Coated Conductors", *Acta. Mater.*, Vol. 49, 2001, pp. 1421-1428.
3. Makita H, Hanada S and Izumi O, *Acta Metall.* Vol. 36, 1988, pp. 403.
4. W.W. Mullins, "Theory of thermal grooving." *J. Appl. Phys.*, vol. 28, 1957, pp. 333-339.
5. T. A. Gladstone, J. C. Moore, A. J. Wilkinson and C. R. M. Grovenor, "Grain boundary misorientation and thermal grooving in cube-textured Ni and Ni-Cr tape",
6. J. Eickemeyer, D. Selbmann, R. Opitz, B. de Boer, B. Holzapfel, L. Schultz and U. Miller, "Nickel-refractory Metal Substrate Tapes With High Cube Texture Stability", *Supercond. Sci. Technol.*, Vol. 14, 2001, pp. 152-159.
7. A. Goyal, R. Feenstra, M. Paranthaman, J.R. Thompson, B.Y. Kang, C. Cantoni, D.F. Lee, F.A. List, P.M. Martin, E. Lara-Curzio, C. Stevens, D.M. Kroeger, M. Kowalewski, E.D. Specht, T. Aytung, S. Sathyamurthy, R.K. Williams, R.E. Ericsson, "Strengthened Biaxially Textured Ni Substrate With Small Alloying Additions for Coated Conductor Applications", *Physica C,* Vol. 382, 2000, pp. 251-262.
8. E. Varesi, V. Boffa, G. Celentano, L. Ciontea, F. Fabbri, V. Galluzzi, U. Gambardella, A. Mancini, T. Petrisor, A. Rufoloni, A. Vannozzi, " Biaxial Texturing of Ni alloy substrate for YBCO Coated Conductors", *Phycica C*, Vol. 372-376, 2002, pp. 763-766.
9. J. Eickemeyer, D. Selbmann, R. Opitz, E. Maher and W. Prusseit, "Highly Cube Textured No-W-RABiTS Tapes for YBCO Coated Conductors", *Phycica C*, Vol. 372-376, 2002, pp. 814-817.

10. J. Knauf, R. Semerad, W. Prusseit, B. de Boer, J. Eickemeyer, *IEEE Trans. Appl. Supercond.* 11 (1) (2001) , 2885–2888.
11. A. Goyal, D.P. Norton, D.M. Kroeger, D.K. Christen, M. Paranthaman, E.D. Specht, *J. Mater. Res.*, V. 12, 1997, pp. 2924.
12. M. W. Rupich, U. Schoop, D. T. Verebelyi, C. Thieme, W. Zhang, X. Li, T. Kodenkandath, N. Nguyen, E. Siegal, D. Buczek, J. Lynch, M. Jowett, E. Thompson, J-S. Wang, J. Scudiere, A. P. Malozemoff, Q. Li, S. Annavarapu, S. Cui, L. Fritzemeier, B. Aldrich, C. Craven, F. Niu, A. Goyal, and M. Paranthaman, "YBCO Coated Conductors", *Applied Superconductivity Conference*, 2002.
13. N. Cheggour, J. W. Ekin, C. C. Clickner, D. T. Verebelyi, C. L. H. Thieme, A. P. Malozemoff, "Transverse Compressive Stress Effect in Y-Ba-Cu-O Coatings on Biaxially Textured Ni and Ni-5at.%W Substrates", *Applied Superconductivity Conference*, 2002.
14. B. De Boer, N. Reger, R. Opitz, J. Eickmeyer, B. Holzapfel and L. Schultz, "Recrystallized Cold Rolled Nickel and Nickel-Alloys With A Strong Cube Texture", Proceedings of the Twelfth International Conference on Texture of Materials, Montreal, Canada, Vol. 2, (Ed.) J.A. Szpunar, pp. 944-949.
15. J.R. Thompson, A. Goyal, D.K. Christen and D.M. Kroeger, "Ni-Cr textured substrates with reduced ferromagnetism for coated conductor applications", *Physica C,* V. 370, 2002, pp. 169-176.
16. G.C. Wood and F.H. Scott, *Mater. Sci. Technol.*, Vol. 3, 1987, pp. 519.
17. A. Tuissi, E. Villa, M. Zamboni, J.E. Evetts, R.I. Tomov, "Biaxially textured NiCrX (X = W and V) tapes as substrates for HTS coated conductor applications", *Physica C*, Vol. 372–376, 2002, pp. 759–762